2013-12-16

Higher-order unfolding of satellite heterochromatin is a consistent and early event in cell senescence

Eric C. Swanson
University of Massachusetts Medical School Worcester

Et al.

Published December 16, 2013

Higher-order unfolding of satellite heterochromatin is a consistent and early event in cell senescence

Eric C. Swanson, Benjamin Manning, Hong Zhang, and Jeanne B. Lawrence

Department of Cell and Developmental Biology, University of Massachusetts Medical School, Worcester, MA 01655

Epigenetic changes to chromatin are thought to be essential to cell senescence, which is key to tumorigenesis and aging. Although many studies focus on heterochromatin gain, this work demonstrates large-scale unraveling of peri/centromeric satellites, which occurs in all models of human and mouse senescence examined. This was not seen in cancer cells, except in a benign senescent tumor in vivo. Senescence-associated distension of satellites (SADS) occurs earlier and more consistently than heterochromatin foci formation, and SADS is not exclusive to either the p16 or p21 pathways. Because Hutchinson Guilford progeria syndrome patient cells do not form excess heterochromatin, the question remained whether or not proliferative arrest in this aging syndrome involved distinct epigenetic mechanisms. Here, we show that SADS provides a unifying event in both progeria and normal senescence. Additionally, SADS represents a novel, cytological-scale unfolding of chromatin, which is not concomitant with change to several canonical histone marks nor a result of DNA hypomethylation. Rather, SADS is likely mediated by changes to higher-order nuclear structural proteins, such as LaminB1.

Introduction

Cultured human primary cells have a limited life span and ultimately become incapable of further division despite remaining metabolically active. This irreversible exit from the cell cycle, widely referred to as cellular senescence, has important implications not only for aging and stem cell biology but also as a key anti-tumorigenesis mechanism. Senescence can be induced by a variety of mechanisms, including shortened telomeres (replicative senescence), oncogene expression, oxidative stress, and replicative exhaustion, or via expression of regulatory factors, such as the ubiquitin ligase SMURF2 (Zhang and Cohen, 2004; Zhang, 2007).

Cellular senescence is accompanied by changes in gene expression and chromatin packaging; however, the absence of cell cycling is the only hallmark that consistently distinguishes senescent cells (Herbig et al., 2004; Cristofalo, 2005; Di Micco et al., 2011; Kosar et al., 2011). Formation of senescence-associated heterochromatic foci (SAHF) has received much attention, not only as a senescence marker but also as a proposed mechanism to promote and stabilize the senescent state (Narita et al., 2003; Zhang et al., 2007). Although SAHF exhibit repressive chromatin modifications, including H3K9Me3, H4 hypoacetylation, macroH2A, and HP1(Adams, 2007), some marks commonly associated with heterochromatin are lost during senescence and aging, such as linker histone H1 and DNA methylation (Funayama et al., 2006; Misteli, 2010).

Although SAHF are common in human senescence, they are not found in all senescent human cells or any senescent mouse cells (Narita et al., 2003; Kennedy et al., 2010). In particular, cells from patients with Hutchinson Guilford progeria syndrome (HGPS) and from aged individuals tend to show loss of visible heterochromatin blocks and associated marks (Shumaker et al., 2006; Misteli, 2010). These inconsistencies leave open the question of whether or not cells in premature aging syndromes such as HGPS undergo the same process for loss of proliferative capacity as normal primary fibroblasts senescing in culture. Furthermore, even within normal cultured senescing fibroblasts it is not known whether SAHF are a key part of the senescence pathway or arise as a consequence of a senescent end state (Narita et al., 2003; Zhang et al., 2007; Kennedy et al., 2010; Di Micco et al., 2011). It would thus be important to identify a broad epigenomic

Correspondence to Jeanne B. Lawrence: jeanne.lawrence@umassmed.edu

Abbreviations used in this paper: 5-AzaC, 5-azacytidine; α-sat, α-satellite; β-gal, β-galactosidase; Chr., chromosome; HGPS, Hutchinson Guilford progeria syndrome; ICF, immunodeficiency, centromeric instability, and facial anomalies; MEF, mouse embryonic fibroblast; PIN, prostatic intraepithelial neoplasia; SADS, senescence-associated distension of satellites; SAHF, senescence-associated heterochromatic foci.

Supplemental Material can be found at:
http://jcb.rupress.org/content/suppl/2013/12/15/jcb.201306073.DC1.html
Original image data can be found at:
http://jcb-dataviewer.rupress.org/jcb/browse/7556

The Rockefeller University Press $30.00
J. Cell Biol. Vol. 203 No. 6 929–942
www.jcb.org/cgi/doi/10.1083/jcb.201306073

Published December 16, 2013

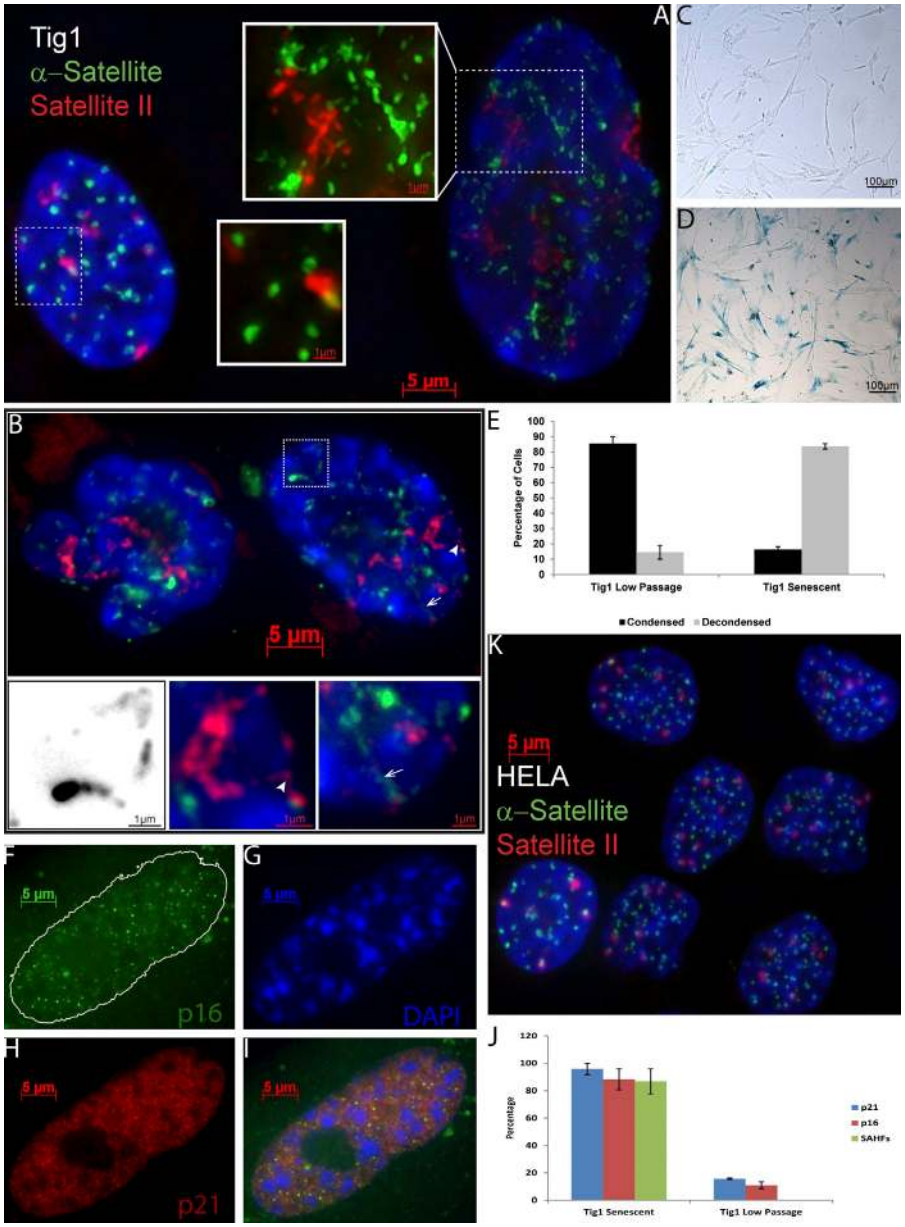

Figure 1. **Satellite DNA signals markedly distend in senescent fibroblasts.** (A) α-Sat (green) and sat II (red) hybridization in early passage culture. Distended satellites are found in a small percentage of nuclei (right; see 3D images and Videos 1 and 2). (B) Most cells in late passage senescent cultures show distended satellites. Note that these cells do not have enlarged nuclei, but contain SAHF (DAPI). Insets show examples of threadlike satellite extensions, some of which extend to and contact the nuclear membrane (indicated by arrows and arrowheads). Inset of boxed region shown in black and white to enhance contrast. (C and D) β-Gal staining confirms that the cycling culture (C) contains few senescent cells and the senescent culture (D) contains many. (E) Quantification showing that senescent cultures contain more cells with distended satellites than cycling cultures. (F–J) Senescence was confirmed by staining for p16 (F), p21 (H), and SAHF (DAPI; G), and quantified (J; error bars are standard error). (K) HeLa cultures do not contain cells with distended satellites.

change to chromatin that consistently occurs during senescence in a variety of human and mouse systems and during premature arrest in cells from patients afflicted by HGPS.

In contrast to the formation of excess facultative heterochromatin, constitutive heterochromatin in senescent cells has received little attention. Here, we demonstrate that the peri/centromeric satellite heterochromatin undergoes a striking decondensation in senescent cells. This dramatic change to structures key to cell division occurs consistently in a variety of senescence models, is not exclusive to either known senescent pathway, and happens independently of and before SAHF formation. It has also been observed in senescent human and mouse cells and appears to be prevalent in vivo in benign prostatic intraepithelial neoplasia (PIN) tumors. Importantly, this change to satellite heterochromatin is particularly prevalent in cultured fibroblasts from two HGPS patients. Thus, what we term senescence-associated distension of satellites (SADS) is a new marker that constitutes an early and potentially key event in the process of cell senescence. We further show that SADS retain several canonical histone hallmarks of heterochromatin, suggesting that this visible unraveling represents change to higher-order chromatin folding potentially at an unprecedented level.

Results

Marked distension of satellite DNA in a subset of primary human fibroblasts

In a culture of proliferative normal diploid fibroblasts (Tig1) hybridized with a probe to α-satellite (α-sat) DNA, we first noted that a small subset of cells appear to have dramatically distended satellites, such that the normally compact round centric-satellite signals (Fig. 1 A, left) form linear extensions that appear "strung out" (Fig. 1 A, right). These thin threads of distended DNA can be difficult to reproduce in print, but were unambiguous through

Published December 16, 2013

the microscope (see online supplemental material). This highly distended pattern was not a sporadic variation peculiar to a few centromeres, but evident in most if not all α-sat signals in a given cell. For quantitative scoring (Fig. 1 E), a cell nucleus had distended satellites when the majority of signals lost their discrete round shape, had threadlike extensions, and elongated along a longitudinal axis. Furthermore, satellite II DNA, found at the pericentromeres of several chromosomes, showed a similarly dramatic loss of its normally tight packaging (Fig. 1 A). Similar patterns were seen in a variety of diploid fibroblast lines including IMR90, WI38, BJ, and LF1, but not in several tumor-derived immortal cell lines. Although some of the fibroblasts with distended satellite DNA had enlarged nuclear morphology (Fig. 1 A, right) others did not (Fig. 1 B); this and other evidence rules out that satellite distention reflects global DNA decondensation throughout the genome.

Satellite distension is a hallmark of cells undergoing replicative senescence in culture

The "fried egg" morphology of some cells with markedly distended satellites in early passage cultures suggested that they may represent senescent primary fibroblasts. Thus we compared early passage, proliferative cultures to those that had undergone replicative senescence. Remarkably, 84% of cells in senescent cultures (Fig. 1, B and E; $n = 3$) had distended α-sat, compared with only 14% of early passage fibroblasts (Fig. 1 E). These cells had several other markers of senescence, including positive senescence-associated β-galactosidase (β-gal) staining, up-regulation of p16 and p21, and often SAHF (Fig. 1, C, D, and F–J). We also examined several transformed cell lines (HeLa, PC3, and U2OS) and despite numerous genetic and epigenetic aberrations in these neoplastic lines we found essentially no cells in these cultures with distended satellite (Fig. 1 K).

Next, to ensure satellite decondensation is not a property of quiescent cells, we examined Tig1 cells serum starved for 48 h or allowed to recover in normal serum for 24 h. Compared with controls, the percentage of cells exhibiting satellite unraveling did not change as a result of serum starvation (Fig. 2 A). Thus, satellite distension is not a property of stressed cells undergoing quiescence, nor a function of general epigenetic aberration in tumor cells, suggesting it is a regulated chromatin change specific to the senescence program.

We also used BrdU incorporation in replicating DNA to discriminate proliferative versus nonproliferative cells, to address whether the ∼15% of cells exhibiting satellite distension in low/mid passage cultures are still cycling or are indeed senescent. A 20-min BrdU pulse in low passage Tig1 fibroblasts demonstrated that the subset of cells exhibiting satellite distension rarely incorporate BrdU (Fig. 2, B–D). As shown in Fig. 2 D, 35.3% of the cells with compact centromeric DNA also labeled with BrdU, whereas <1% (0.64%) had both BrdU and decondensed satellite, demonstrating that cells with satellite distension do not simultaneously replicate DNA. Similar results were seen in late passage fibroblasts (five passages from full senescence; Fig. 2 E). We then used a 48-h BrdU pulse to ask what percentage of senescent cells (defined by lack of DNA replication over 2 d) exhibit satellite distension. Importantly, in both early and late passage cultures, almost all BrdU-negative cells had decondensed satellite DNA, indicating this is a consistent change characteristic of senescent cells (Fig. 2 F).

Exposing cells to BrdU for a long period (48 h) is helpful to mark cells that are no longer cycling, but is long enough that some cells could label during their last S phase and then withdraw from the cell cycle. This would occur more frequently in late passage cultures in which many cells are entering senescence. Consistent with this, of the 15% of early passage cells that contained distended satellite DNA (Fig. 2 D), only 1.8% of these also incorporated BrdU during the 48-h label (Fig. 2 G). In contrast, in late passage, rapidly senescing cultures, ∼25% of cells had distended satellites (Fig. 2 E) and up to 38% of these also labeled with BrdU (Fig. 2 G). This difference was observed in multiple experiments and suggests that within 48 h of the last DNA replication, cells entering senescence have already undergone major structural changes to satellite DNA. To test this further, the 48-h label was done on a fully senescent culture; in this case ∼85% of cells had distended satellites, but only 6% of these stained positive for BrdU (Fig. 2 G).

SADS is a hallmark of senescence induced by SMURF2 expression, oxidative stress, or oncogenic Ras

We next addressed whether SADS occur in human cells induced to senesce via mechanisms that do not include telomere shortening (replicative senescence), thus we tested this in cells induced to senesce by three other methods: overexpression of SMURF2, oxidative stress, and oncogenic Ras. Previous work has shown that up-regulation of the ubiquitin ligase SMURF2 induces early onset senescence in cycling fibroblasts (Zhang and Cohen, 2004). Subsequently, several days after infection with SMURF2, cultures were largely senescent as judged by the presence of SADS (Fig. 3, A, B, E, and F), SAHF (Fig. 3, E and F; and Fig. S1 C), and β-gal staining (Fig. S1, A and B). Importantly, in multiple experiments the majority of infected cells (up to 90%) exhibited satellite distension within 10 d, whereas cells infected with a control vector did not (Fig. 3, E and F). Additionally, we induced early passage Tig1 fibroblasts to senesce by either oxidative stress or overexpression of oncogenic Ras, and subsequently observed that neither culture became confluent, many cells contained SAHF, and 73% and 71% of the cells had distended satellites, respectively (Fig. 3, C and D). These findings show that satellite distension is not exclusive to replicative senescence, but can be induced fairly rapidly by expression of the senescence regulator SMURF2, through oxidative stress or oncogenic Ras.

Satellite distension is not exclusive to either p21 or p16 senescence pathways

Previous work has revealed two pathways that fibroblasts use to undergo senescence, either the p53/p21 or p16/Rb (Zhang, 2007). Interestingly, cells do not up-regulate both p21 and p16 until late in senescence (Herbig et al., 2004). Although SAHF formation occurs primarily via the p16 pathway, cells such as BJ fibroblasts, which lack significant p16 expression, do not form SAHF (Narita et al., 2003; Fig. 3, A and B; and Fig. S1 C). Thus it was important

Published December 16, 2013

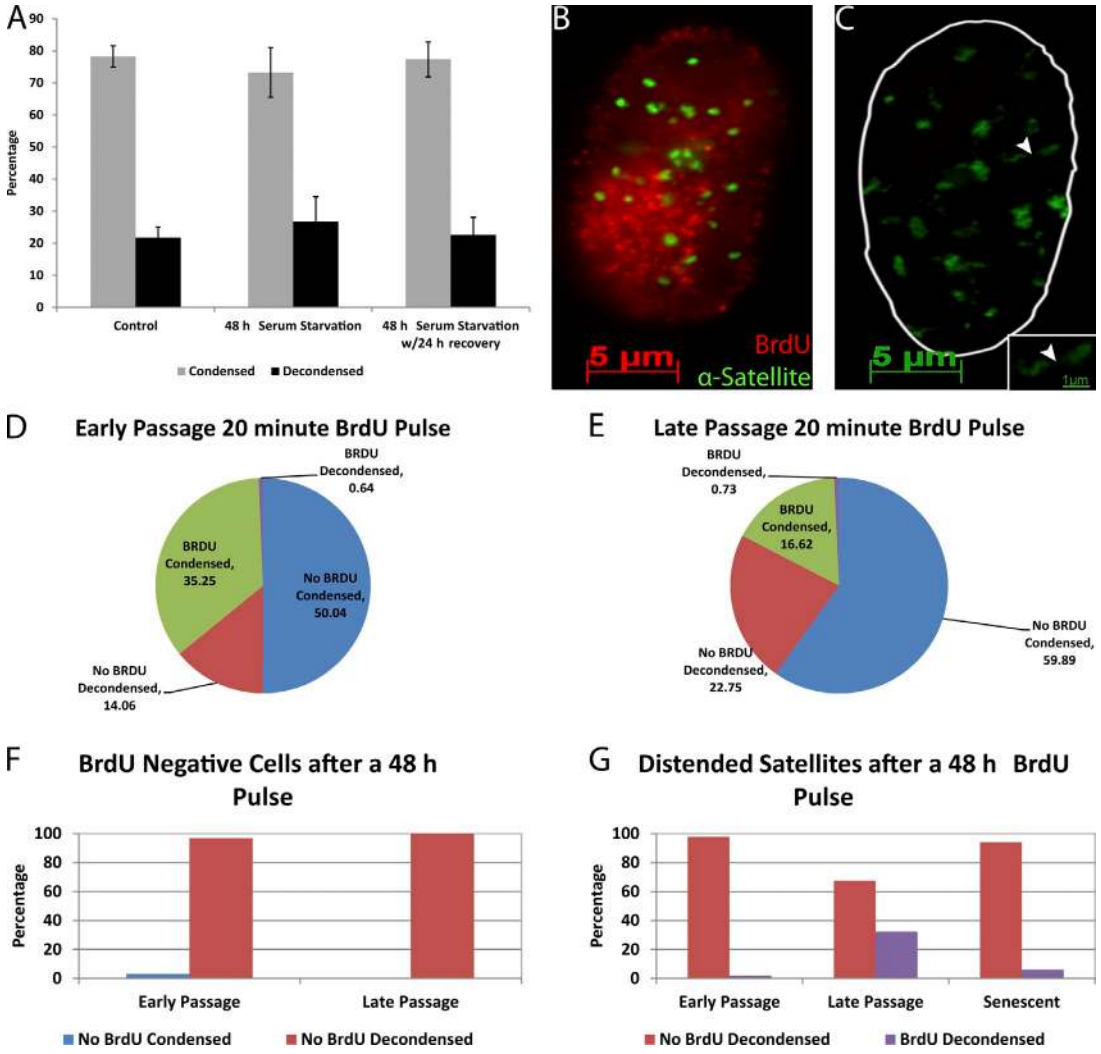

Figure 2. **BrdU labeling demonstrates that distended satellites are characteristic of and specific to senescent fibroblasts.** (A) Satellites do not distend in quiescent, serum-starved cells. (B and C) BrdU (red) labels cells with condensed satellites (green; B) but not cells with decondensed satellites (C). Inset shows high magnification of a distended satellite (arrowhead; cells are from same field). (D and E) Quantification of satellite distension in early (D) and late (E) passage cultures subjected to a 20-min BrdU pulse, confirming that cells with decondensed satellites are rarely in S phase. (F) Almost all cells that did not incorporate BrdU during a 48-h pulse had distended satellites (n = 100–200, from one of three repeats). (G) Early passage and senescent cells with distended satellites rarely incorporate BrdU during the previous 48-h period (n = 100–200, representative of one of three repeats). In presenescent late passage cultures in which more cells are entering senescence, a significant fraction of cells with distended satellites incorporated BrdU (error bars represent standard error).

to address whether satellite distension is specific to one of these pathways or is a more consistent event that can occur by either pathway. We began by performing p21 staining together with DNA FISH to α-sat in late passage Tig1 fibroblasts, using an antibody confirmed to show p21-specific staining (Fig. S1, D and E). Interestingly, some cells with distended satellites expressed high levels of p21 (56%), whereas others expressed little or none (Fig. 3 G). To further validate that SADS can occur before or independent of p21 expression, we examined p21 knockout LF1 fibroblasts, which showed distended satellites in 86% of cells, similar to the frequency in normal senescent Tig1 fibroblasts (Fig. 3, H–J; Fig. 1 B; and Fig. S1 I). This supports that SADS can occur independent of the p21 pathway.

Because SADS do not require p21, they may occur via the p16 pathway, but a distinct question is whether p16 is required. When we used SMURF2 to induce senescence in BJ fibroblasts, satellite distension was only slightly reduced compared with SMURF2-induced LF1 senescent fibroblasts (Fig. 3, E and F). Although there is a near complete loss of SAHF in BJ cells that lack substantial p16 expression, SADS are still highly prevalent. As further evidence that SADS do not require p16 we examined p16 null mammary epithelial cells, which also formed distended satellites (Fig. S1, F–I). Hence, SADS does not require p16 and is not restricted to either of the two established senescence pathways.

Satellite distension is an early event in senescence and independent of SAHF formation

Several observations support that SADS occurs early in cell senescence, well before and independent of SAHF formation. As shown in Fig. 3 (A and B), we observed cells with decondensed

Published December 16, 2013

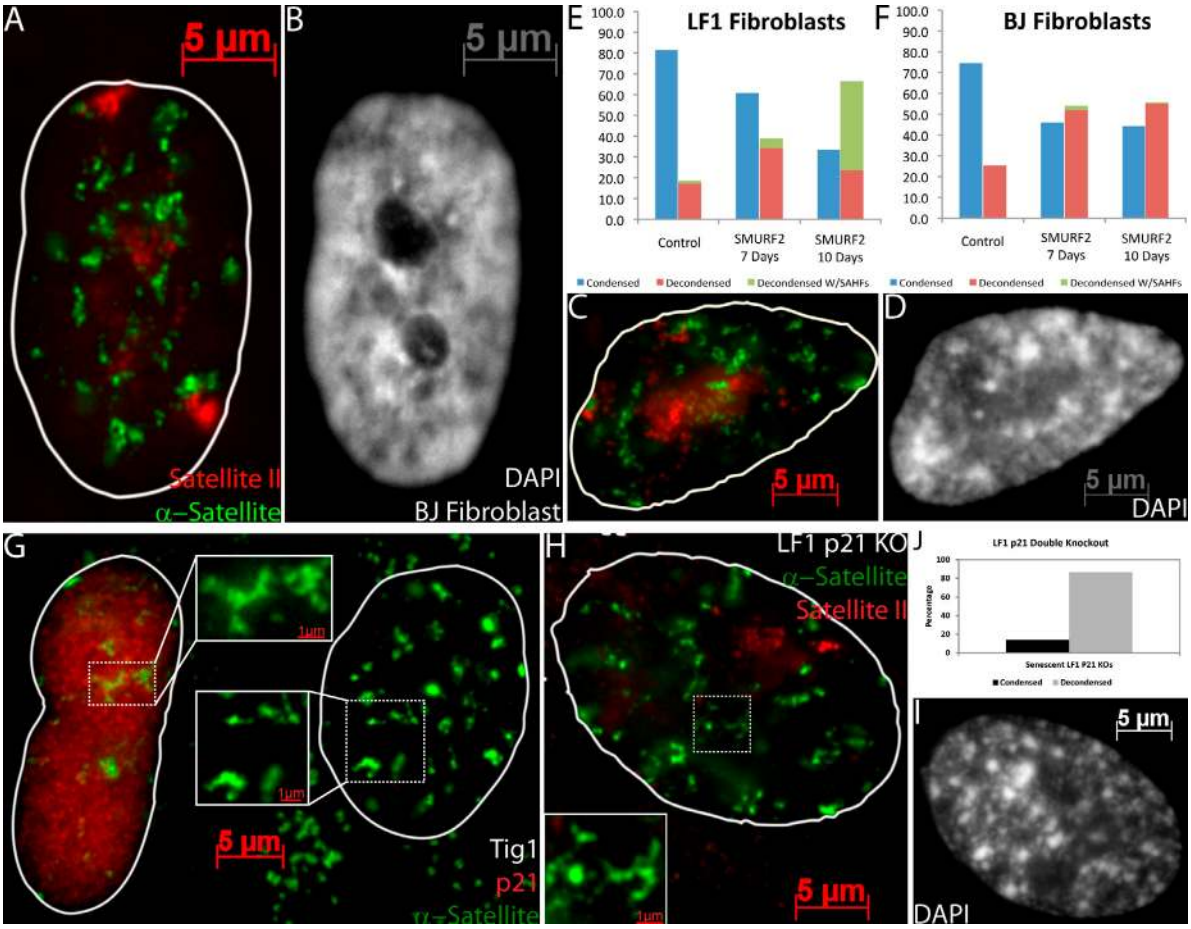

Figure 3. **SADS is a property common to multiple different senescence models and pathways.** (A and B) SADS is present in a SMURF2-induced senescent BJ fibroblast, yet these cells do not form SAHF (B). (C and D) Oxidative stress-induced senescence of a Tig1 fibroblast results in distension of α-sat (green) and sat II (red) in a cell with SAHF (DAPI; D). (E and F) Quantification of SADS and SAHF in LF1 and BJ fibroblasts, induced with wild-type SMURF2 (n = 200, representative of one of three repeats). (G) Tig1 fibroblasts with SADS (green) may or may not be positive for p21 staining (red). (H–J) SADS in LF1 p21 knockout cells are quantified (n = 204; J) and a SAHF-positive senescent cell is shown (H and I) with α-sat (green), sat II (red), and DAPI (I).

satellites and no SAHF, but the opposite was never true. Furthermore, SAHF formation is very uncommon in BJ fibroblasts with low p16 expression, but SADS still occurs after SMURF2-induced senescence (Fig. 3, A, B, and F; and Fig. S1 C). Further evidence that SADS occurs before SAHF formation came from LF1 cells transfected with SMURF2. Just 2 d after selection of SMURF2 expressing cells, only 5% had SAHF, whereas 39% had SADS. By 5 d, more cells had SAHF (48%) but still more had SADS (67%; Fig. 3 E and Fig. S1 C). As such, satellite decondensation appears to occur irrespective of and before SAHF formation in all senescent fibroblasts examined.

SADS occurs in senescent murine cells and in vivo in a human benign tumor

Our findings show that senescence of normal human cells in vitro involves not only gain of facultative heterochromatin (SAHF) but also breakdown of constitutive heterochromatin (SADS), which is a consistent and early hallmark of senescence. Given the differences between human and mouse senescence (Itahana et al., 2004; Kennedy et al., 2010), it would be significant if SADS constitutes a hallmark common to both species. As such, we tested the universality of SADS by examining senescent cultures of normal mouse embryonic fibroblasts (MEFs). In many of these cells, the normally round chromocenters, organized clusters of the pericentric major satellite visible by DAPI staining, did indeed show structural aberrations (Fig. 4, B and D) exemplified by irregular shapes that coalesced, frequently with fibrous interconnections. In situ hybridization to the smaller blocks of minor satellite DNA (the centromere proper) demonstrated that 86% of cells in a culture of senescent MEFs (Fig. 4 E, β-gal staining) no longer formed small, round, and compact signals (Fig. 4 A, top), but clearly was extended, irregular, and often threadlike (Fig. 4, A–C). Therefore, SADS is a prominent chromatin change common to both mouse and human senescence.

Because some markers of human senescence, including SAHF, have not been verified in vivo (Kreiling et al., 2010), we obtained sections of premalignant PIN tissue (Fig. 4, F and G) known to have high levels of senescence (Chen et al., 2005). We then used β-gal staining to verify the presence of senescence in this tissue (Fig. 4 H) and DNA FISH to α-sat and sat II sequences in serial sections to reveal that distended satellite signals are present in cells within the positive β-gal–stained regions of PIN tissue (Fig. 4, I and J). In contrast, examination of tissue sections from several malignant cancers that lack senescent cells, including

Published December 16, 2013

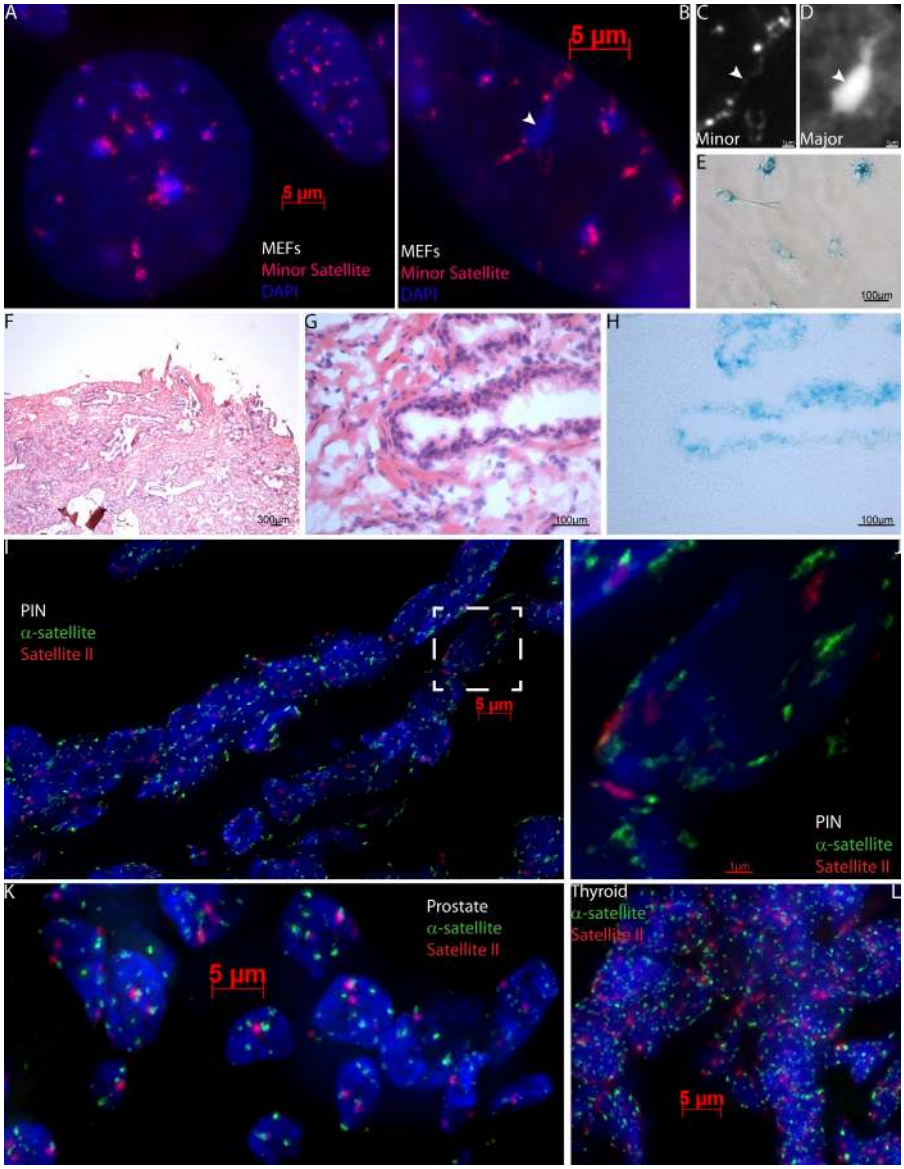

Figure 4. **SADS occur in MEFs and senescent cells within human tumors.** (A) Cycling MEFs (top right) have condensed minor satellite (red), whereas senescent MEFs (bottom left) have distended minor satellite. (B–D) A senescent MEF with coalesced and elongated chromocenters (DAPI) and stringy minor satellite (red). The arrowhead points to a particularly elongated chromocenter (D) associated with a highly decondensed minor satellite (C). (E) Senescent MEFs, as shown in B, stain positive for β-gal. (F–J) Serial sections reveal SADS in PIN tissue. Using H&E staining (F and magnified in G) to identify PIN, which contains senescent cells as indicated by positive β-gal staining (H) and distended satellites by α-sat (green) and sat II (red; I). Signals from I (white box) are enlarged in J. (K and L) Malignant prostate (K) and thyroid (L) tumors, which lack senescent cells, typically have round, compact signals of α-sat (green) and sat II (red).

breast, thyroid, pancreatic, and prostate, showed that the satellites were condensed (Fig. 4, K and L; and not depicted), demonstrating that only in the senescent PIN tumor were there large sections of cells with distended satellites, which indicates that SADS are an in vivo marker characteristic of senescent cells.

SADS occurs in HGPS patient cells undergoing premature proliferative arrest

We next addressed whether SADS would also be seen in cells of patients with a devastating human disease that is an important model of in vivo aging—HGPS. HGPS patients express a mutated form of lamin A/C that causes global defects in the nuclear heterochromatic compartment. Consistent with the rapid aging phenotype, HGPS cells undergo premature senescence in culture, providing an in vitro model for human aging. However, neither in vivo nor in vitro do HGPS cells exhibit gain of visible heterochromatin blocks (SAHF) or heterochromatic marks. Instead, a general decrease in H3K9me3, HP1, and NURD-associated factors has been reported (Scaffidi and Misteli, 2006; Shumaker et al., 2006; Pegoraro et al., 2009). This apparent contradiction leaves open the question of whether HGPS cells undergo proliferative arrest by mechanisms distinct from senescence in normal cells. Therefore, we obtained primary HGPS skin fibroblasts to examine if satellite distension is evident in these cells as they arrest. We examined three different early passage cultured fibroblast lines: a 1-yr-old male (HGADFN155 passage 10, PD 21), an 8-yr-old female (HGADFN167 passage 11, PD 20), and that female's 37-yr-old healthy biological mother (HGMDFM090 passage 13, PD 23). This demonstrated that although a fraction of cells had compact satellites (Fig. 5, A and E), satellite distension is indeed a hallmark of many cultured HGPS cells (Fig. 5, A, D, and F). For example, almost 50% of the 1-yr-old boy's cells, which displayed a marked HGPS phenotype (blebbed and contorted nuclei), had distended satellites. Additionally, cells with SADS were confirmed to be noncycling by a 20-min BrdU pulse in the 8-yr-old girl's cell line, with just 1.5% of total cells having both SADS and BrdU label versus 29% with SADS and no BrdU (Fig. 5 B). We then asked

Published December 16, 2013

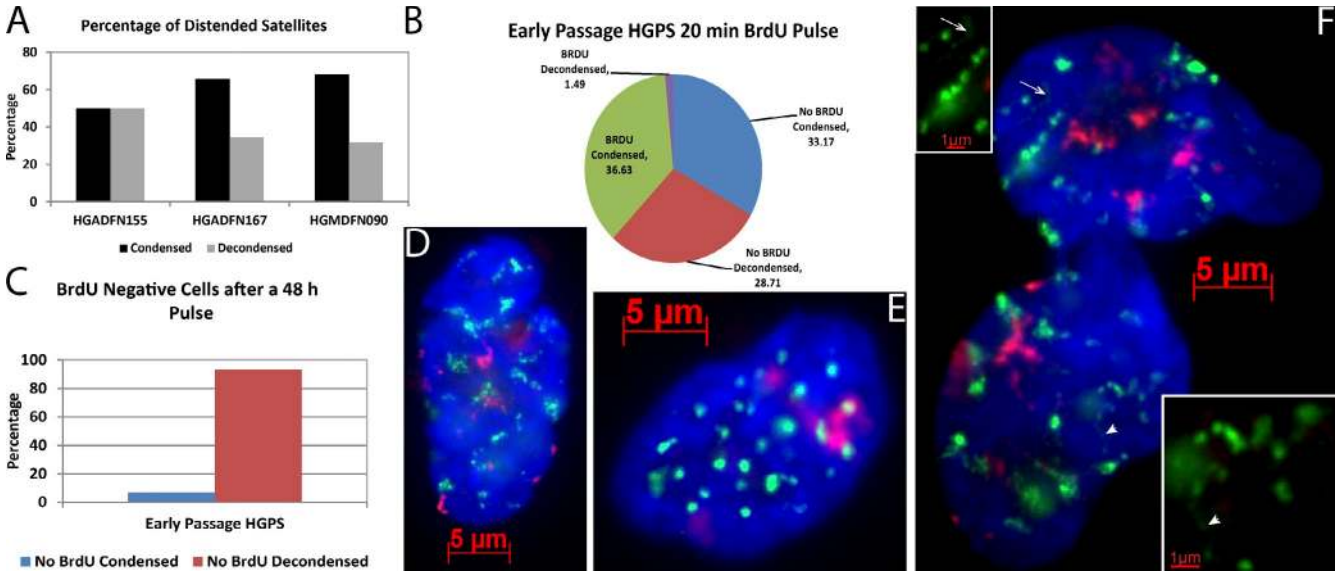

Figure 5. **SADS is characteristic of HGPS cells that undergo premature arrest.** (A) Frequency of distended satellites in early passage cells from two HGPS patients (1-yr-old HGADFN155 and 8-yr-old HGADFN167) and the older healthy mother of HGADFN167, HGMDFM090 (n = 100 in one of three representative experiments). (B) A 20-min BrdU pulse demonstrates that very few early passage HGADFN167 cells with decondensed satellites label, confirming that cells with SADS are rarely in S phase (n = 202). (C) Almost all cells that did not incorporate BrdU during a 48-h label had distended satellites (n = 100). (D–F) DNA FISH to α-sat (green) and sat II (red) shows that some HGPS cells have normal appearing compact satellites (E), whereas senescent cells in both the HGADFN167 (D) and HGADFN155 (F) cell lines contain SADS. Also notice the blebbed nuclear membrane (DAPI; F) characteristic of laminopathies. Arrows and arrowheads indicate a particularly distended α-sat signal that is enlarged in the corresponding insets.

if cells that failed to incorporate BrdU after 48 h had visibly distended satellites, and similar to normal senescing cultures almost all did (Fig. 5 C). These findings reinforce that a high fraction of HGPS cells have removed themselves from the cell cycle despite the young age and early passage of these cultures. Most importantly, the prevalence of SADS indicates that this premature proliferative arrest shares a fundamental epigenomic change with replicative as well as induced senescence of normal human and mouse cells.

SADS is a unique higher-order unfolding of chromatin distinct from DNA decondensation linked to expression

Several aspects of our findings suggest that SADS represents a unique change to higher-order chromatin folding, of a much different nature than in other studies of DNA decondensation. Changes in DNA condensation are known to be linked to active chromatin and certain histone modifications, but such molecular-scale changes are below the resolution of light microscopy and can only be determined by techniques such as DNase sensitivity. In contrast, SADS can be readily seen despite the limited resolution of light microscopy. To address whether SADS is linked to expression of the corresponding satellite sequences, we examined satellite RNA expression in senescence cells using well established techniques (Lawrence et al., 1989). In primary normal fibroblasts with visible SADS, sat II RNA is not substantially expressed (see Fig. 7, A and B) despite the dramatic decondensation of the DNA. In contrast, we and others have shown that sat II RNA is highly expressed in many rapidly cycling cancer cells (Ting et al., 2011; unpublished data), including cancer cell lines that we show have tightly packaged satellite DNA signals (Fig. 1 K and see Fig. 7 F). Thus, visible satellite distension was not related to satellite RNA expression.

To quantify the extent of this striking satellite distension, we measured the signal using a probe specific to the α-sat on human chromosome 17 (Chr. 17), in proliferative versus senescent Tig1 fibroblasts. The Chr. 17 α-sat in senescent, SAHF-positive Tig1 fibroblasts had a mean length of 5.44 µm, in contrast to 0.88 µm in cycling cells (Fig. 6, A–E). As shown in Fig. 6 D, the shortest Chr. 17 satellite signal in SAHF-positive cells was more extended than the largest found in cycling cells. This increased satellite length does not merely reflect changes in nuclear size because large cycling nuclei with condensed satellites were observed as well as small nuclei with decondensed satellites (Fig. 1 B) and mean satellite length increased over sixfold, whereas nuclear diameter increased slightly less than twofold (Fig. 6, C and E). In addition, the signal size of a randomly selected 156-kb BAC (containing the Chr. 21 Dyrk1 locus) showed no decondensation in senescent cells (Fig. 6, F–H), and there was no visible difference in the condensation of traditionally heterochromatic telomere signals in senescent (SMURF2 induced) and nonsenescent control cells (Fig. 6, I–L). Hence, satellite distension is not merely a reflection of nuclear size nor indiscriminate chromatin decondensation.

Satellite unfolding occurs on chromatin that retains canonical histone marks of heterochromatin

Because SADS represents such a marked change in chromatin packaging, we anticipated that heterochromatin-associated modifications and possibly centromere-specific CENP proteins would change dramatically. We found that both CENP-A and -B

Published December 16, 2013

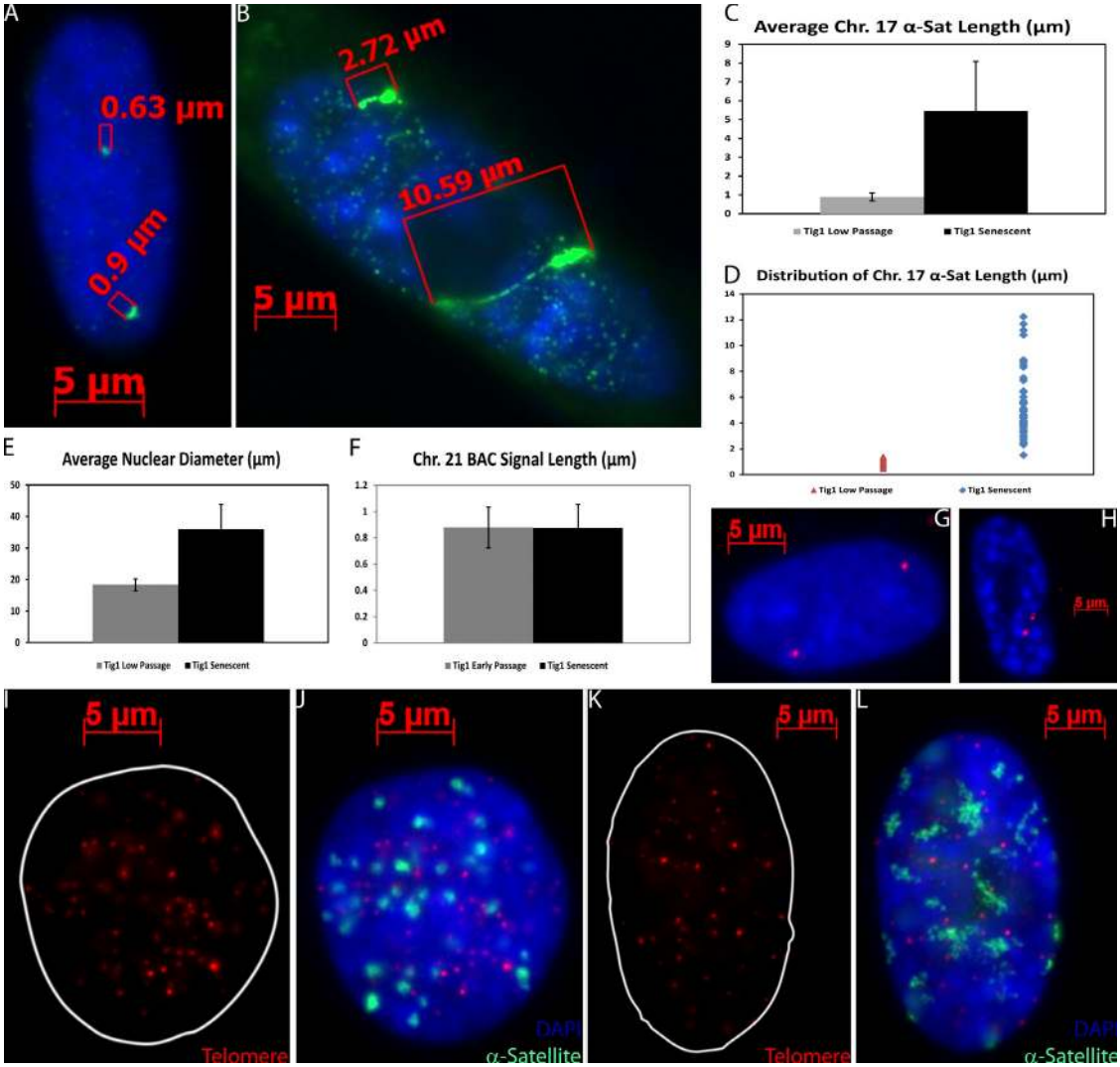

Figure 6. **Loss of compaction is specific to satellite DNA and is not caused by increased nuclear size.** (A and B) DNA FISH to Chr. 17 α-sat (green) shows compact satellite signals in a cycling cell (A) and distended satellites in a senescent cell (B) as determined by the presence of SAHF (DAPI). The size of the corresponding signal is shown above the brackets. (C) The mean length of Chr. 17 α-sat in senescent cells is six times the mean length in cycling cells. (D) The shortest Chr. 17 α-sat measured in senescent cells is longer than the largest satellite measured in cycling cells. (E–H) Differences in satellite length cannot be explained by the twofold increase in nuclear diameter (E). The mean size of the Chr. 21 BAC signal (red) did not change (F) in cycling (G) or senescent (H) cells. (I–L) Telomere signal size (red) in cycling (I and J) or SMURF2-induced senescent (K and L) LF1 cells did not change. Senescence is judged by distension of the α-sat (green) and presence of SAHF (DAPI; error bars represent standard error).

still associate with distended satellites in senescent cells. Consistent with CENP-B remaining bound across the broader segment of α-sat DNA, the normally compact CENP-B signal becomes visibly decondensed in senescent cells (Fig. 7 C and Fig. S2, A and B). In contrast, CENP-A, which binds to the much smaller α-sat core, was not visibly distended (Fig. S2, A and B, see linescans comparing CENP-A and -B). Although CENP-A is still present, it did appear dimmer in many (but not all) senescent cells, consistent with a recent report of overall lower CENP-A levels in senescent cells (Maehara et al., 2010).

We next examined several heterochromatin modifications typically associated with DNA condensation, which we anticipated to be depleted from highly distended satellite DNA, such as linker histone H1, which has been shown to decrease during senescence (Funayama et al., 2006). We noted that in cells with SADS 64% still had high levels of H1, suggesting that nuclear H1 depletion occurs after SADS form, consistent with other evidence that this H1 loss is concomitant with SAHF formation (Fig. S3, D–F). We and others also noted that SAHF stain strongly for repressive heterochromatin marks H3K9me3 and HP1γ (Narita et al., 2003; Zhang et al., 2005), and the accumulation of these marks on SAHF is concomitant with sharply lower levels of H3K9me3 and HP1γ in nucleoplasmic regions between SAHF, where the distended satellites reside (Fig. 1 B; Fig. S3, A–C; and Fig. S4 C; Funayama et al., 2006). Although SADS had formed in many cells that had clearly not redistributed H3K9Me3 (Fig. S3, B and C), the threadlike nature of SADS makes it difficult to determine by molecular cytology if the canonical heterochromatin marks (H3K9Me3 and H3K27Me3) are still on the DNA.

Therefore, to address H3K9Me3 and H3K27Me3 distribution at higher resolution, we analyzed the α-sat sequences for

Published December 16, 2013

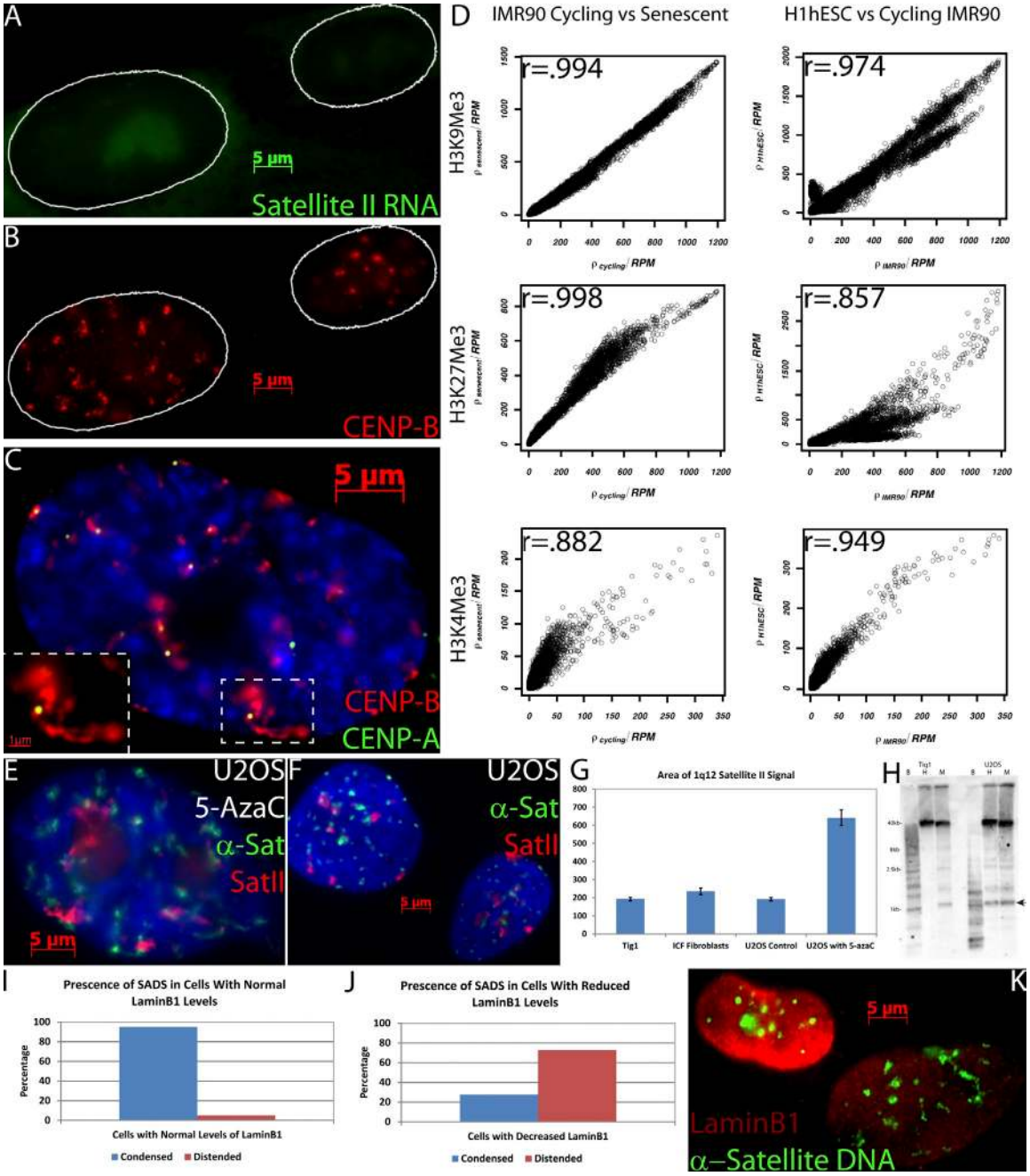

Figure 7. **Analysis of expression, heterochromatin proteins, DNA methylation, and histone modifications in satellites.** (A and B) FISH to sat II RNA (green) shows no increased expression with SADS formation in senescent (left) versus cycling (right) cells, with satellite chromatin marked by CENP-B staining (red). (C) CENP-A (green) and CENP-B (red) are still present in senescent cells as determined by the presence of SAHF (DAPI) and decondensed CENP-B staining (magnified in inset). (D) Comparison of H3K9me3, H3K27me3, and H3K4me3 read densities between cycling and senescent IMR90 cells and between cycling IMR90 and H1hES cells on α-sat (RepeatMasker class: HSATII) sequences with corresponding Pearson's r values. (E and F) As all cancer samples examined, U2OS cells have compact satellites (F; α-sat, green; sat II, red) and do not form SADS unless treated with 5-AzaC, which induces senescence (E). (G) Quantification of mean 1q12 signal areas ($n > 60$) in different cell samples (error bars represent standard error). (H) A DNA methylation-sensitive Southern blot with U2OS and cycling Tig1 cells digested by BstB1 (B), HpaII (H), or MspI (M) and detected with a probe for sat II 1q12 sequences. The arrow points to a band size that is lacking in some of the methylation-sensitive HpaII lanes, indicating that the 1q12 region is methylated in the corresponding cell types. (I–K) Cells with normal levels of LaminB1 (red; top left) rarely contain distended α-sat (green; I and K), but in cells with SADS (bottom right) LaminB1 is often diminished (J and K; $n = 100$ from one of three replicates).

these histone modifications, using publically available ChIP-seq data (Chandra et al., 2012). Surprisingly, the number of reads in α-sat sequences for heterochromatin marks H3K9Me3 and H3K27Me3 was tightly correlated in cycling and senescent cells, indicating that there was not a change in the level of these marks despite satellite distension (Fig. 7 D). These observations are in stark contrast to the differences in these histone modifications on satellite DNA between undifferentiated ES cells and cycling IMR-90 fibroblasts (Fig. 7 D) even though the packaging of these satellites remains visibly unchanged (not depicted).

Published December 16, 2013

We then examined the histone modification H3K4Me3, which is associated with gene expression, and noticed that levels of this mark changed slightly between both cycling and senescent cells and less so between ES and cycling fibroblasts (Fig. 7 D). Collectively, these results indicate that SADS formation involves higher-order unfolding of satellite chromatin that does not require changes in canonical histone marks associated with condensed heterochromatin (H3K9Me3 and H3K27Me3) or decondensed euchromatin (H3K4Me3).

We also considered whether loss of DNA methylation could trigger SADS formation. Interestingly, hypomethylation of satellite DNA is prevalent in most cancer samples (Ehrlich, 2009), yet the 13 different cancer samples (cell lines and tumors) examined here did not exhibit SADS (with the exception of the senescent benign PIN tissue). Surprisingly, we noted that 5-azacytidine (5-AzaC) induced SADS in U20S cancer cells after several days of treatment (Fig. 7, E–G). However, these cells no longer cycled, presumably because 5-AzaC is known to induce senescence in normal and cancer cells through activation of the p16/INK4a promoter (which is often hypermethlyated in cancer; Fang et al., 2004; Schnekenburger et al., 2011). To validate the interpretation that SADS formation after 5-AzaC treatment was a result of senescence, rather than a direct result of DNA hypomethylation, we examined untreated U2OS cells by a DNA methylation-sensitive Southern blot that confirmed that untreated U2OS sat II at 1q12 was hypomethylated (Fig. 7 H). In contrast, cycling Tig1 fibroblasts had methylated satellites as expected (and results suggest little or no change to satellite methylation upon senescence; Fig. 7 H and Fig. S5 D). Further evidence that DNA demethylation does not cause SADS came from examination of α-sat and sat II 1q12 in fibroblasts from a patient with immunodeficiency, centromeric instability, and facial anomalies (ICF) syndrome (Fig. S5, A and B), a disease characterized by a lack of DNA methylation on 1q12 caused by a mutation in DNA methytransferase3b (Ehrlich et al., 2008). Measurement of sat II DNA 1q12 signals in interphase nuclei showed at most a very slight increase and was similar to normal fibroblasts or untreated U2OS cells (Fig. 7, E–G; and Fig. S5, B and C). Similarly, the α-sat signals did not show significant distension (Fig. S5 A). Collectively, these results indicate that the striking unfolding of satellite heterochromatin within nuclei of noncycling cells is tightly linked to cell senescence and is not triggered by DNA hypomethylation.

The magnitude of satellite DNA distension described here suggests that senescence likely involves changes to nuclear structural proteins that play a role in higher-order folding of the chromatin fiber. In this context, it is significant that we show a prevalence of SADS in HGPS cells (Fig. 5), considering that defects in lamina have been shown to have an impact in the nuclear organization of centromeric satellites (Taimen et al., 2009), that lamina-associated domains are enriched in pericentric satellite DNA (Guelen et al., 2008), and that SADS frequently extend along the nuclear periphery or stretch from central regions all the way to the lamina (e.g., Figs. 1 B, 6 B, and S5 C). Recent work also shows marked decreases in LaminB1 levels in both HGPS and normal cell senescence (Shimi et al., 2011; Freund et al., 2012). Consequently, we performed α-sat DNA FISH and antibody staining to LaminB1 in mid passage WI-38 fibroblasts and found that 95% of cells with normal LaminB1 levels had condensed satellites (Fig. 7, I and K). In contrast, in cells with obviously depleted LaminB1 staining, 73% had clearly distended satellites (Fig. 7, J and K; and Fig. S2, C and D). As further considered in the Discussion, this suggests that changes in LaminB1 and potentially other nuclear structural proteins may contribute to higher-order unraveling of satellite DNA during senescence.

Discussion

Epigenetic changes to chromatin are thought key to senescence and have received substantial attention; however, this study demonstrates a prominent, genome-wide chromatin change that has eluded discovery and runs counter to expectations that senescence is marked primarily by gain of large blocks of heterochromatin. We reveal that large-scale distension or "unraveling" of centric and pericentric satellite heterochromatin is a distinguishing mark of senescent cells that occurs in all senescence models studied here, with both high sensitivity and specificity. Furthermore, this distension occurs early in the senescence process and, unlike SAHF formation, is not exclusive to either the p16 or p21 senescence pathways.

Although SADS occurs earlier and more consistently than SAHF formation, that both occur in the same senescent nuclei resolves the seemingly incompatible or paradoxical findings regarding gain versus loss of heterochromatin marks in senescent and aged cells (Funayama et al., 2006; Narita et al., 2006; Scaffidi and Misteli, 2006; Kreiling et al., 2010; Kosar et al., 2011). Our findings clearly show that loss of constitutive heterochromatin and gain of facultative heterochromatin occurs in the same nucleus. Although bright accumulations of many heterochromatin marks, such as H3K9me3 or HP1γ, become prominent in senescent cells, the whole nucleus does not gain these heterochromatin marks; rather, senescence is characterized by redistribution of condensed and decondensed genomic regions.

A unifying epigenetic feature of all senescence models examined including mouse and HGPS

An important point demonstrated here is that SADS occurs during permanent cell cycle withdrawal for all of many different cell types and methods examined to induce cell senescence. Human cells that lack SAHF (BJ fibroblasts) still form SADS but, more importantly, SADS bridges what has been a major gap between mouse and human cell senescence: both the major and minor satellites distend with threadlike extensions in senescent MEFs. This clarifies our previous observation that the chromocenters of Dicer-depleted MEFs, which senesce prematurely, lost their round compact shape and appeared to connect and coalesce (Mudhasani et al., 2008). Additionally, we observed distended satellite heterochromatin in senescent cells within PIN cancer tissues, which is significant because other heterochromatin changes (SAHF) have not been observed in vivo (Kreiling et al., 2010).

Published December 16, 2013

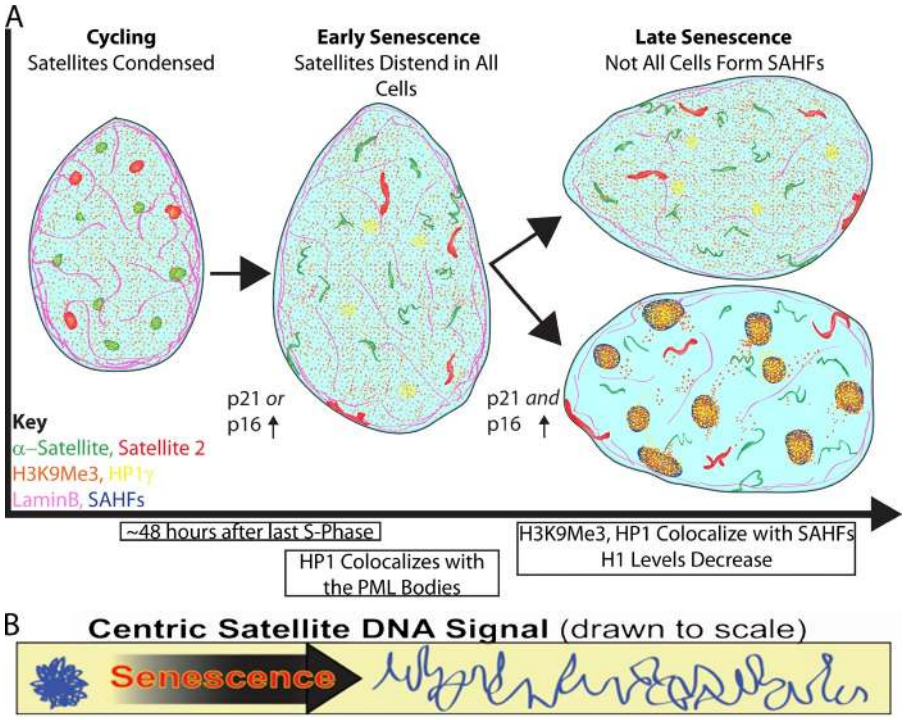

Figure 8. **Satellite distension in relation to other events in the cell senescence process.** (A) In nuclei of cycling cells, the peri/centromeric satellite DNA signals are tightly compacted, but dramatically distend in senescent cells. This occurs before and irrespective of the later formation of SAHF, and in some cells within 48 h of the last S phase. SADS is seen in essentially all noncycling cells and occurs in cells that first up-regulate either the p21 or p16 pathway. In late stage senescence, both pathways are up-regulated, and the p16 pathway promotes formation of SAHF. During this process there is a reorganization of several heterochromatin factors as seen by immunofluorescence including H3K9Me3 and HP1γ, whereas H1 levels uniformly decrease with the formation of SAHF. Whereas nuclear diameter increases progressively and is most pronounced in cells with SAHF, SADS are seen in some cells before nuclear enlargement. The nuclear lamina protein (LaminB1) may play a role in the higher-order folding of the DNA as it is diminished in most cells before SADS form. (B) Sat DNA in cycling cells is tightly packaged and this packaging is lost during senescence as the DNA distends. Because three canonical histone modifications remain unchanged during senescence the difference in DNA packaging may be attributed to changes in higher-order folding.

The importance of SADS providing a unifying theme of senescent cells is especially evident in relation to the debate regarding HGPS. Interestingly, HGPS cells do not exhibit increases in repressive marks typical of normal senescent fibroblasts; rather they show depletion of repressive factors (Scaffidi and Misteli, 2005; Shumaker et al., 2006). Thus there has been a lingering question as to whether chromatin changes in HGPS cells reflect mechanisms of cell cycle arrest that are fundamentally distinct from that of normal cell senescence. Importantly, early passage fibroblasts from two young HGPS patients undergoing proliferative arrest showed a high rate of SADS. Therefore, this marked distension of satellites constitutes a more universal epigenetic program that underlies the biology of both HGPS and normal cell senescence.

Integration of SADS into the senescence process: A model

Fig. 8 A provides an overview of SADS formation relative to several changes characteristic of senescent cells. Multiple points of evidence demonstrate that unraveling of compact satellite DNA is a relatively early step, and the rapid nature with which SADS occurs contrasts sharply with the broader changes to chromatin seen by FAIRE analysis 3–4 mo after entry into senescence (De Cecco et al., 2013). For example, BrdU labeling of cultures nearing senescence showed satellite distension present in cells within 48 h of the last S phase. SADS are often evident before SAHF formation, but never vice versa, and similarly, SADS can be observed before nuclear enlargement. As previously reported (Herbig et al., 2004) and indicated by results here, early in senescence cells often express either p21 or p16, but not both, but we see SADS irrespective of which pathway may trigger senescence. SADS could also be seen in cells that were not yet depleted for histone H1, which is consistent with other evidence that loss of H1 is a late event (Funayama et al., 2006). Additionally, many nuclei containing SADS had not redistributed heterochromatin marks (H3K9Me3 and HP1γ) onto SAHF. Hence, our model conveys that satellite DNA distension occurs before and irrespective of a more global redistribution of facultative heterochromatin.

SADS is large-scale chromatin unfolding facilitated by nuclear structural proteins rather than histone modifications

We have referred to the changes in satellite packaging reported here, and modeled in Fig. 8 B, as distension rather than decondensation to emphasize that the change in packaging is on a different scale then the decondensation that has been widely studied in the control of gene expression. To our knowledge, such a marked extension of chromatin in an interphase nucleus is relatively unique in biology and may be unprecedented. That a single centromeric α-sat was often as long as 5 µm (Fig. 6) suggests that these α-sat blocks (ranging from ∼0.5 to 3 Mb) exhibit significant decompaction ∼5× below the level of condensed chromatin and lower than levels seen in a large genic locus (Lawrence et al., 1990). This clearly cytological scale distension, coupled with the surprising finding that the DNA is still packaged in nucleosomes that retain three canonical histone marks (Fig. 7 D), leads us to propose that SADS involves changes of higher-order chromatin loops, such as release of satellite DNA from scaffolding and other chromosomal structural proteins, rather than modifications of core histones.

Given that HGPS is caused by mutations in LaminA/C and is characterized by higher levels of SADS, and that LaminB1 is depleted in HGPS and senescent normal fibroblasts, an important possibility is that changes to these scaffold proteins could play a role in satellite distension (Shimi et al., 2011;

Published December 16, 2013

Freund et al., 2012). Although our evidence indicates that cells with SADS do not always have low LaminB1 staining, SADS did not appear to occur in cells that have high LaminB1 staining (Fig. 8 A, model). Therefore, LaminB1 may be one of several proteins that anchor satellite heterochromatin in nuclei and its loss may contribute to increased destabilization of satellite architecture and subsequent higher-order unfolding of DNA.

Potential implications of SADS for cell cycle withdrawal

This discovery raises the possibility that the early unraveling of satellite heterochromatin could contribute to permanent cell cycle withdrawal. In this context, it is interesting to note that the cell cycle regulator Rb has been reported to interact with the nuclear lamina and play a role in the stabilization of satellite heterochromatin (Gonzalo and Blasco, 2005; Dorner et al., 2007; Marji et al., 2010). In addition, various other components of the interphase centromere/kinetochore could be impacted; for example, CENP-F, which interacts with Rb and blocks cells at the G1–S transition (Du et al., 2010), or CENP-G, which associates with α-sat throughout the cell cycle and may interact with the nuclear matrix (He et al., 1998).

Hence, the discovery of SADS provides the field with a prominent, early, and consistent marker of senescence, and is likely to spark new avenues of research into how unraveling of interphase centromeres arises. SADS also helps to resolve a paradox between the loss of heterochromatin reported within some aging and senescence models and the gain of heterochromatin reported in others by showing that all cell types studied here consistently lose higher-order folding in satellite DNA. Finally, the magnitude of centromeric heterochromatin distension revealed here opens new avenues of inquiry into higher-order chromatin packaging, as well as its relationship to cell senescence.

Materials and methods

Cell culture

Lung fibroblasts including Tig1, WI-38, and IMR-90 (Coriell) as well as ICF cells (GM08747; Coriell) were grown in MEM containing 15% FBS. LF1 and BJ fibroblasts, LF1 p21 knockouts, and HGPS cell lines (The Progeria Research Foundation) were grown in DMEM containing 15% FBS. MEFs (a gift from D. Carone, University of Massachusetts Medical School, Worcester, MA) and neoplastic cancer lines (PC3, HELA, and U2OS; American Type Culture Collection) were grown in DMEM with 10% FBS. 48R human mammary epithelial cells (from normal female breast tissues) were maintained in mammary epithelial cell growth medium. Cells were passaged 1:2 when cultures reached confluency. Cultures were defined as senescent when they failed to reach confluency 10 d after a 1:2 split. Oxidative stress was induced by treating early passage confluent Tig1 fibroblasts with 250 µM H_2O_2 for 2 h. The cells were allowed to recover for 2 d before they were replated on coverslips and fixed after 6 d. SMURF2-induced senescent cells (LF1 and BJ fibroblasts) were transfected and selected before being replated onto coverslips and fixed either 7 or 10 d after transfection (Zhang and Cohen, 2004). For Ras-induced senescence, Tig1 cells were infected with ocogenic ras or control retrovirus containing a puro selection marker overnight, allowed to recover for 24 h, selected for 3 d, and allowed to recover for 3 d before being plated on coverslips and fixed the following day.

Cell and tissue preparation for in situ hybridization or immunoflourescence

Cells were extracted in CSK buffer with 0.5% Triton X-100 for 3–5 min and fixed in 4% PFA for 10 min (Johnson et al., 1991a). Cells used for p16, p21, and LaminB1 staining were fixed before Triton X-100 extraction. SADS were observed independent of fixation technique. Prepared cells were stored in 70% ethanol until use. Tissues were acquired from the University of Massachusetts Cancer Center Tissue Bank and fixed in the same manner as the cells.

In situ DNA and RNA hybridization

For DNA hybridizations, cells were denatured for 2 min at 75°C and then hybridized with biotin or direct labeled oligos (Lawrence et al., 1988). Oligos were hybridized in 15% formamide. The Chr. 21 BAC containing the DYRK1 gene, the Chr. 17–specific α-sat, and the satellite II 1q12 probes were nick translated and hybridized in 50% formamide (Johnson et al., 1991b). In addition, some senescent cells were denatured for 2–6 min to increase signal intensity and hybridization efficiency. Tissues were denatured for 10–15 min. Oligo sequences were α-sat (FITC direct label, 5′-CTTTTGATAGAGCAGTTTTGAAACACTCTTTTTGTAGAATCTGCAAGTGGATATTTGG-3′), sat II (LNA, biotin, 5′-ATTCCATTCAGATTCCATTCGATC-3′), and mouse minor satellite (equal parts biotin labeled, 5′-GAACAGTGTATATCAATGAGTTAC-3′ and 5′-CCACACTGTAGAACATATTAGATG-3′).

Immunofluorescence and cell staining

Cells were incubated with antibodies at 1:250 dilution in PBS 1% BSA at 37°C for 1 h. Slides were rinsed in PBS, PBS with 0.01% Triton X-100, and PBS again for 10 min each before detection. Antibodies included p16 (Abcam), p21 (Santa Cruz Biotechnology, Inc.), CENP-A (Abcam), CENP-B (Santa Cruz Biotechnology, Inc.), HP1γ (EMD Millipore), H3K9Me3 (EMD Millipore), LaminB1 (Santa Cruz Biotechnology, Inc.), and H1 (a gift from M. Bustin, Texas Woman's University, Denton, TX). In cells with both antibodies and in situ hybridizations to α-sat DNA, the DNA hybridization was performed first, followed by antibody staining. Slides were stained with DAPI for 30 s and mounted with Vectashield media.

BrdU labeling and in situ hybridization was performed on nonconfluent Tig1 fibroblasts using 30 µM BrdU. They were extracted, fixed, denatured, and hybridized with an α-sat probe (as described in "In situ DNA and RNA hybridization") and incubated with a BrdU antibody (Partec) at a 1:200 dilution and washed before detection as described earlier. Finally, senescence-specific β-gal staining was performed according to Dimri et al. (1995).

Image analysis

The threadlike satellite sequences may be hard to see in print but were unmistakable through the microscope. As such, sections of images were often magnified for reader convenience and we encourage the viewing of our images in a digital format. We performed the imaging using an Axiovert 200 or an Axiophot microscope (Carl Zeiss) equipped with a 100× PlanApo objective (NA 1.4) and Chroma 83000 multi-bandpass dichroic and emission filter sets, set up in a wheel to prevent optical shift. Images were captured with a camera (Orca-ER) or a 200 series CCD camera (Photometrics) using AxioVison 4.8 software (Carl Zeiss). Z stacks were a compilation of 15–30 images taken at an interval of 0.1 to 0.25 µm, and subsequent image deconvolution was done using AxioVision 3D software theoretical PSF (Carl Zeiss) and either the nearest neighbor or fast iterative algorithm. Distances were measured using either Axiovision 4.8 or MetaMorph 4.6 software. Most experiments were performed a minimum of three times and scored by at least two independent investigators. All findings were easily visible by eye through the microscope (unless otherwise noted).

Analysis of ChIP-seq data

Publicly available ChIP-seq data (Chandra et al., 2012) were collected and analyzed. ChIP-seq and input sequence reads were mapped to the GRCh37.p11 (hg19) reference genome using bowtie (v. 0.2.8; Langmead et al., 2009) and read densities and regions of statistically significant enrichment ("peaks") were determined using model-based analysis of ChIP-Seq (v. 1.4.1; Zhang et al., 2008) using default settings. Tandem repeat sequences in hg19 were annotated using RepeatMasker (Smit and Green, 1996–2010). For the purposes of visualization, read densities were normalized by scaling such that mean read densities for common ChIP-seq peaks were equal to one another, similar to the approach of MAnorm (Shao et al., 2012). The RepeatMasker α-sat sequences were divided into 100-bp fragments over which the mean normalized read densities were compared.

Western blots

35 µg of each lysate was run over 15% SDS-PAGE and electroblotted onto 0.2 µm of immunoblot PVDF (Bio-Rad Laboratories) for 90 min at 350 mA, 4°C. Western analysis was performed in PBS and 0.1% Tween 20, with or without 5% nonfat dry milk powder as necessary. Antibody concentrations

and incubations are as follows: 1:500 rabbit α-p16 overnight at 4°C, 1:1,000 mouse α-p21 overnight at 4°C, 1:8,000 mouse α-tubulin 1 h at room temp, 1:1,000 HRP goat α-mouse (Thermo Fisher Scientific) 1 h at room temp, and 1:1,000 HRP α-rabbit (GE Healthcare) 2 h at room temperature.

Methylation-sensitive Southern blots

Cells were pelleted and resuspended in 50 µl of lysis buffer (400 mM Tris-Cl, 60 mM EDTA, 150 mM NaCl, and 1% SDS), incubated with RNase for 30 min at 37°C, treated with ProK overnight at 50°C, and then subjected to a phenol chloroform extraction. 10 µg of DNA was then digested overnight with HpaII, MspI, or BstB1 (New England Biolabs, Inc.) and run on a 1% agarose gel. DNA was transferred overnight to a nylon membrane using capillary action and fixed with 0.4 M NaOH. DNA of interest was detected using the Bright Star Biodetect kit (Ambion) with a nick-translated biotin-labeled probe for sat II 1q12 (prepared as described in "In situ DNA and RNA hybridization"). The membrane was imaged with Chemidoc (Bio-Rad Laboratories).

Online supplemental material

Videos 1 and 2 show a moving 3D rendering and a movie of each slice in the Z stack of Fig. 1 A. Fig. S1 reinforces that SADS are a property common to multiple different senescence models and pathways. Fig. S2 shows the CENP-A and -B distribution on individual centromeres of senescent cells as well as LaminB1 levels in cycling and senescent cells. Figs. S3 and S4 use immunofluorescence to illustrate changes in H3K9Me3, H1, and HP1γ during senescence. Fig. S5 further addresses the effects of 5-AzaC and hypomethylation on satellite distension. Online supplemental material is available at http://www.jcb.org/cgi/content/full/jcb.201306073/DC1. Additional data are available in the JCB DataViewer at http://dx.doi.org/10.1083/jcb.201306073.dv.

We would like to acknowledge members of the Lawrence laboratory, especially D. Carone and L. Hall, for their assistance with many aspects of this project; T.W. Whitfield for his expertise in carrying out the bioinformatics analysis to generate results in Fig. 7 D; and H. Kolpa for editing. We would also like to thank members of the H. Zhang laboratory for their expertise with various aspects of this work. Finally, we would like to thank A. Fischer, S. Lyle, and the University of Massachusetts Cancer Center Tissue Bank for their assistance with acquiring and analyzing the tissues.

Funding for this work was provided by J. Lawrence (RO1 GM053234).

Submitted: 13 June 2013
Accepted: 13 November 2013

References

Adams, P.D. 2007. Remodeling of chromatin structure in senescent cells and its potential impact on tumor suppression and aging. *Gene*. 397:84–93. http://dx.doi.org/10.1016/j.gene.2007.04.020

Chandra, T., K. Kirschner, J.-Y. Thuret, B.D. Pope, T. Ryba, S. Newman, K. Ahmed, S.A. Samarajiwa, R. Salama, T. Carroll, et al. 2012. Independence of repressive histone marks and chromatin compaction during senescent heterochromatic layer formation. *Mol. Cell*. 47:203–214. http://dx.doi.org/10.1016/j.molcel.2012.06.010

Chen, Z., L.C. Trotman, D. Shaffer, H.-K. Lin, Z.A. Dotan, M. Niki, J.A. Koutcher, H.I. Scher, T. Ludwig, W. Gerald, et al. 2005. Crucial role of p53-dependent cellular senescence in suppression of Pten-deficient tumorigenesis. *Nature*. 436:725–730. http://dx.doi.org/10.1038/nature03918

Cristofalo, V.J. 2005. SA beta Gal staining: biomarker or delusion. *Exp. Gerontol.* 40:836–838. http://dx.doi.org/10.1016/j.exger.2005.08.005

De Cecco, M., S.W. Criscione, E.J. Peckham, S. Hillenmeyer, E.A. Hamm, J. Manivannan, A.L. Peterson, J.A. Kreiling, N. Neretti, and J.M. Sedivy. 2013. Genomes of replicatively senescent cells undergo global epigenetic changes leading to gene silencing and activation of transposable elements. *Aging Cell*. 12:247–256. http://dx.doi.org/10.1111/acel.12047

Di Micco, R., G. Sulli, M. Dobreva, M. Liontos, O.A. Botrugno, G. Gargiulo, R. dal Zuffo, V. Matti, G. d'Ario, E. Montani, et al. 2011. Interplay between oncogene-induced DNA damage response and heterochromatin in senescence and cancer. *Nat. Cell Biol.* 13:292–302. http://dx.doi.org/10.1038/ncb2170

Dimri, G.P., X. Lee, G. Basile, M. Acosta, G. Scott, C. Roskelley, E.E. Medrano, M. Linskens, I. Rubelj, O. Pereira-Smith, et al. 1995. A biomarker that identifies senescent human cells in culture and in aging skin in vivo. *Proc. Natl. Acad. Sci. USA*. 92:9363–9367. http://dx.doi.org/10.1073/pnas.92.20.9363

Dorner, D., J. Gotzmann, and R. Foisner. 2007. Nucleoplasmic lamins and their interaction partners, LAP2α, Rb, and BAF, in transcriptional regulation. *FEBS J.* 274:1362–1373. http://dx.doi.org/10.1111/j.1742-4658.2007.05695.x

Du, J., Y. Li, and X. Zhu. 2010. Involvement of CENP-F in histone methylation. *Acta Biochim. Biophys. Sin. (Shanghai)*. 42:173–176. http://dx.doi.org/10.1093/abbs/gmq001

Ehrlich, M. 2009. DNA hypomethylation in cancer cells. *Epigenomics*. 1:239–259. http://dx.doi.org/10.2217/epi.09.33

Ehrlich, M., C. Sanchez, C. Shao, R. Nishiyama, J. Kehrl, R. Kuick, T. Kubota, and S.M. Hanash. 2008. ICF, an immunodeficiency syndrome: DNA methyltransferase 3B involvement, chromosome anomalies, and gene dysregulation. *Autoimmunity*. 41:253–271. http://dx.doi.org/10.1080/08916930802024202

Fang, J.Y., L. Yang, H.Y. Zhu, Y.X. Chen, J. Lu, R. Lu, Z.H. Cheng, and S.D. Xiao. 2004. 5-Aza-2′-deoxycytidine induces demethylation and up-regulates transcription of p16INK4A gene in human gastric cancer cell lines. *Chin. Med. J. (Engl.)*. 117:99–103.

Freund, A., R.-M. Laberge, M. Demaria, and J. Campisi. 2012. Lamin B1 loss is a senescence-associated biomarker. *Mol. Biol. Cell*. 23:2066–2075. http://dx.doi.org/10.1091/mbc.E11-10-0884

Funayama, R., M. Saito, H. Tanobe, and F. Ishikawa. 2006. Loss of linker histone H1 in cellular senescence. *J. Cell Biol.* 175:869–880. http://dx.doi.org/10.1083/jcb.200604005

Gonzalo, S., and M.A. Blasco. 2005. Role of Rb family in the epigenetic definition of chromatin. *Cell Cycle*. 4:752–755. http://dx.doi.org/10.4161/cc.4.6.1720

Guelen, L., L. Pagie, E. Brasset, W. Meuleman, M.B. Faza, W. Talhout, B.H. Eussen, A. de Klein, L. Wessels, W. de Laat, and B. van Steensel. 2008. Domain organization of human chromosomes revealed by mapping of nuclear lamina interactions. *Nature*. 453:948–951. http://dx.doi.org/10.1038/nature06947

He, D., C. Zeng, K. Woods, L. Zhong, D. Turner, R.K. Busch, B.R. Brinkley, and H. Busch. 1998. CENP-G: a new centromeric protein that is associated with the alpha-1 satellite DNA subfamily. *Chromosoma*. 107:189–197. http://dx.doi.org/10.1007/s004120050296

Herbig, U., W.A. Jobling, B.P.C. Chen, D.J. Chen, and J.M. Sedivy. 2004. Telomere shortening triggers senescence of human cells through a pathway involving ATM, p53, and p21(CIP1), but not p16(INK4a). *Mol. Cell*. 14:501–513. http://dx.doi.org/10.1016/S1097-2765(04)00256-4

Itahana, K., J. Campisi, and G.P. Dimri. 2004. Mechanisms of cellular senescence in human and mouse cells. *Biogerontology*. 5:1–10. http://dx.doi.org/10.1023/B:BGEN.0000017682.96395.10

Johnson, C.V., J.A. McNeil, K.C. Carter, and J.B. Lawrence. 1991a. A simple, rapid technique for precise mapping of multiple sequences in two colors using a single optical filter set. *Genet. Anal. Tech. Appl.* 8:75–76. http://dx.doi.org/10.1016/1050-3862(91)90052-S

Johnson, C.V., R.H. Singer, and J.B. Lawrence. 1991b. Fluorescent detection of nuclear RNA and DNA: implications for genome organization. *Methods Cell Biol.* 35:73–99. http://dx.doi.org/10.1016/S0091-679X(08)60569-5

Kennedy, A.L., T. McBryan, G.H. Enders, F.B. Johnson, R. Zhang, and P.D. Adams. 2010. Senescent mouse cells fail to overtly regulate the HIRA histone chaperone and do not form robust Senescence Associated Heterochromatin Foci. *Cell Div.* 5:16. http://dx.doi.org/10.1186/1747-1028-5-16

Kosar, M., J. Bartkova, S. Hubackova, Z. Hodny, J. Lukas, and J. Bartek. 2011. Senescence-associated heterochromatin foci are dispensable for cellular senescence, occur in a cell type- and insult-dependent manner and follow expression of p16(ink4a). *Cell Cycle*. 10:457–468. http://dx.doi.org/10.4161/cc.10.3.14707

Kreiling, J.A., M. Tamamori-Adachi, A.N. Sexton, J.C. Jeyapalan, U. Munoz-Najar, A.L. Peterson, J. Manivannan, E.S. Rogers, N.A. Pchelintsev, P.D. Adams, and J.M. Sedivy. 2010. Age-associated increase in heterochromatic marks in murine and primate tissues. *Aging Cell*. 10:292–304. http://dx.doi.org/10.1111/j.1474-9726.2010.00666.x

Langmead, B., C. Trapnell, M. Pop, and S.L. Salzberg. 2009. Ultrafast and memory-efficient alignment of short DNA sequences to the human genome. *Genome Biol.* 10:R25. http://dx.doi.org/10.1186/gb-2009-10-3-r25

Lawrence, J.B., C.A. Villnave, and R.H. Singer. 1988. Sensitive, high-resolution chromatin and chromosome mapping in situ: presence and orientation of two closely integrated copies of EBV in a lymphoma line. *Cell*. 52:51–61. http://dx.doi.org/10.1016/0092-8674(88)90530-2

Lawrence, J.B., R.H. Singer, and J.A. McNeil. 1990. Interphase and metaphase resolution of different distances within the human dystrophin gene. *Science*. 249:928–932. http://dx.doi.org/10.1126/science.2203143

Lawrence, J.B., K. Taneja, and R.H. Singer. 1989. Temporal resolution and sequential expression of muscle-specific genes revealed by in situ hybridization. *Dev. Biol.* 133:235–246. http://dx.doi.org/10.1016/0012-1606(89)90314-X

Maehara, K., K. Takahashi, and S. Saitoh. 2010. CENP-A reduction induces a p53-dependent cellular senescence response to protect cells from executing

defective mitoses. *Mol. Cell. Biol.* 30:2090–2104. http://dx.doi.org/10.1128/MCB.01318-09

Marji, J., S.I. O'Donoghue, D. McClintock, V.P. Satagopam, R. Schneider, D. Ratner, H.J. Worman, L.B. Gordon, and K. Djabali. 2010. Defective lamin A-Rb signaling in Hutchinson-Gilford Progeria Syndrome and reversal by farnesyltransferase inhibition. *PLoS ONE*. 5:e11132. http://dx.doi.org/10.1371/journal.pone.0011132

Misteli, T. 2010. Higher-order genome organization in human disease. *Cold Spring Harb. Perspect. Biol.* 2:a000794. http://dx.doi.org/10.1101/cshperspect.a000794

Mudhasani, R., Z. Zhu, G. Hutvagner, C.M. Eischen, S. Lyle, L.L. Hall, J.B. Lawrence, A.N. Imbalzano, and S.N. Jones. 2008. Loss of miRNA biogenesis induces p19Arf-p53 signaling and senescence in primary cells. *J. Cell Biol.* 181:1055–1063. http://dx.doi.org/10.1083/jcb.200802105

Narita, M., M. Narita, V. Krizhanovsky, S. Nuñez, A. Chicas, S.A. Hearn, M.P. Myers, and S.W. Lowe. 2006. A novel role for high-mobility group a proteins in cellular senescence and heterochromatin formation. *Cell*. 126:503–514. http://dx.doi.org/10.1016/j.cell.2006.05.052

Narita, M., S. N□nez, E. Heard, M. Narita, A.W. Lin, S.A. Hearn, D.L. Spector, G.J. Hannon, and S.W. Lowe. 2003. Rb-mediated heterochromatin formation and silencing of E2F target genes during cellular senescence. *Cell*. 113:703–716. http://dx.doi.org/10.1016/S0092-8674(03)00401-X

Pegoraro, G., N. Kubben, U. Wickert, H. Göhler, K. Hoffmann, and T. Misteli. 2009. Ageing-related chromatin defects through loss of the NURD complex. *Nat. Cell Biol.* 11:1261–1267. http://dx.doi.org/10.1038/ncb1971

Scaffidi, P., and T. Misteli. 2005. Reversal of the cellular phenotype in the premature aging disease Hutchinson-Gilford progeria syndrome. *Nat. Med.* 11:440–445. http://dx.doi.org/10.1038/nm1204

Scaffidi, P., and T. Misteli. 2006. Lamin A-dependent nuclear defects in human aging. *Science*. 312:1059–1063. http://dx.doi.org/10.1126/science.1127168

Schnekenburger, M., C. Grandjenette, J. Ghelfi, T. Karius, B. Foliguet, M. Dicato, and M. Diederich. 2011. Sustained exposure to the DNA demethylating agent, 2′-deoxy-5-azacytidine, leads to apoptotic cell death in chronic myeloid leukemia by promoting differentiation, senescence, and autophagy. *Biochem. Pharmacol.* 81:364–378. http://dx.doi.org/10.1016/j.bcp.2010.10.013

Shao, Z., Y. Zhang, G.C. Yuan, S.H. Orkin, and D.J. Waxman. 2012. MAnorm: a robust model for quantitative comparison of ChIP-Seq data sets. *Genome Biol.* 13:R16. http://dx.doi.org/10.1186/gb-2012-13-3-r16

Shimi, T., V. Butin-Israeli, S.A. Adam, R.B. Hamanaka, A.E. Goldman, C.A. Lucas, D.K. Shumaker, S.T. Kosak, N.S. Chandel, and R.D. Goldman. 2011. The role of nuclear lamin B1 in cell proliferation and senescence. *Genes Dev.* 25:2579–2593. http://dx.doi.org/10.1101/gad.179515.111

Shumaker, D.K., T. Dechat, A. Kohlmaier, S.A. Adam, M.R. Bozovsky, M.R. Erdos, M. Eriksson, A.E. Goldman, S. Khuon, F.S. Collins, et al. 2006. Mutant nuclear lamin A leads to progressive alterations of epigenetic control in premature aging. *Proc. Natl. Acad. Sci. USA*. 103:8703–8708. http://dx.doi.org/10.1073/pnas.0602569103

Smit, A.F.A., R. Hubley, and P. Green. 1996–2010. RepeatMasker Open-3.0. http://www.repeatmasker.org (accessed on July 1, 2013).

Taimen, P., K. Pfleghaar, T. Shimi, D. Möller, K. Ben-Harush, M.R. Erdos, S.A. Adam, H. Herrmann, O. Medalia, F.S. Collins, et al. 2009. A progeria mutation reveals functions for lamin A in nuclear assembly, architecture, and chromosome organization. *Proc. Natl. Acad. Sci. USA*. 106:20788–20793. http://dx.doi.org/10.1073/pnas.0911895106

Ting, D.T., D. Lipson, S. Paul, B.W. Brannigan, S. Akhavanfard, E.J. Coffman, G. Contino, V. Deshpande, A.J. Iafrate, S. Letovsky, et al. 2011. Aberrant overexpression of satellite repeats in pancreatic and other epithelial cancers. *Science*. 331:593–596. http://dx.doi.org/10.1126/science.1200801

Zhang, H. 2007. Molecular signaling and genetic pathways of senescence: its role in tumorigenesis and aging. *J. Cell. Physiol.* 210:567–574. http://dx.doi.org/10.1002/jcp.20919

Zhang, H., and S.N. Cohen. 2004. Smurf2 up-regulation activates telomere-dependent senescence. *Genes Dev.* 18:3028–3040. http://dx.doi.org/10.1101/gad.1253004

Zhang, R., W. Chen, and P.D. Adams. 2007. Molecular dissection of formation of senescence-associated heterochromatin foci. *Mol. Cell. Biol.* 27:2343–2358. http://dx.doi.org/10.1128/MCB.02019-06

Zhang, R., M.V. Poustovoitov, X. Ye, H.A. Santos, W. Chen, S.M. Daganzo, J.P. Erzberger, I.G. Serebriiskii, A.A. Canutescu, R.L. Dunbrack, et al. 2005. Formation of MacroH2A-containing senescence-associated heterochromatin foci and senescence driven by ASF1a and HIRA. *Dev. Cell*. 8:19–30. http://dx.doi.org/10.1016/j.devcel.2004.10.019

Zhang, Y., T. Liu, C.A. Meyer, J. Eeckhoute, D.S. Johnson, B.E. Bernstein, C. Nusbaum, R.M. Myers, M. Brown, W. Li, and X.S. Liu. 2008. Model-based analysis of ChIP-Seq (MACS). *Genome Biol.* 9:R137. http://dx.doi.org/10.1186/gb-2008-9-9-r137

Swanson et al., http://www.jcb.org/cgi/content/full/jcb.201306073/DC1

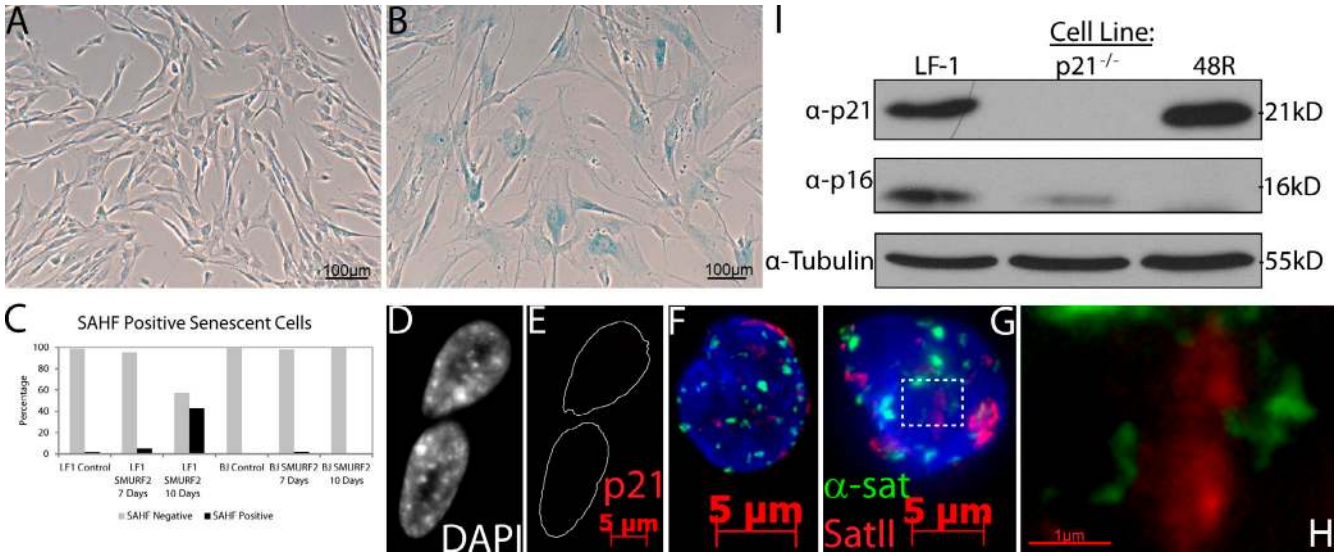

Figure S1. **SADS is a property common to many different senescence models and pathways.** (A and B) β-Gal staining shows that LF1 fibroblasts infected with SMURF2 (B) are senescent, whereas cells infected with a control (A) are not. (C) Percentage of BJ and LF1 cells with SAHF plotted as an independent variable (n = 200, representative of one of three repeats). (D and E) p21 staining (red) is not present in LF1 p21 knockout senescent cells as judged by the presence of SAHF (DAPI; negative antibody control). (F–H) SADS form in human breast epithelial p16 knockout cells as judged by distended α-sat (green) and sat II (red; G) and blown up in H, while others have tight satellite signals indicative of cycling cells (F). (I) Western blot demonstrating that senescent LF1 $p21^{-/-}$ and 48R mammary epithelial cells lack p21 and p16 expression, respectively.

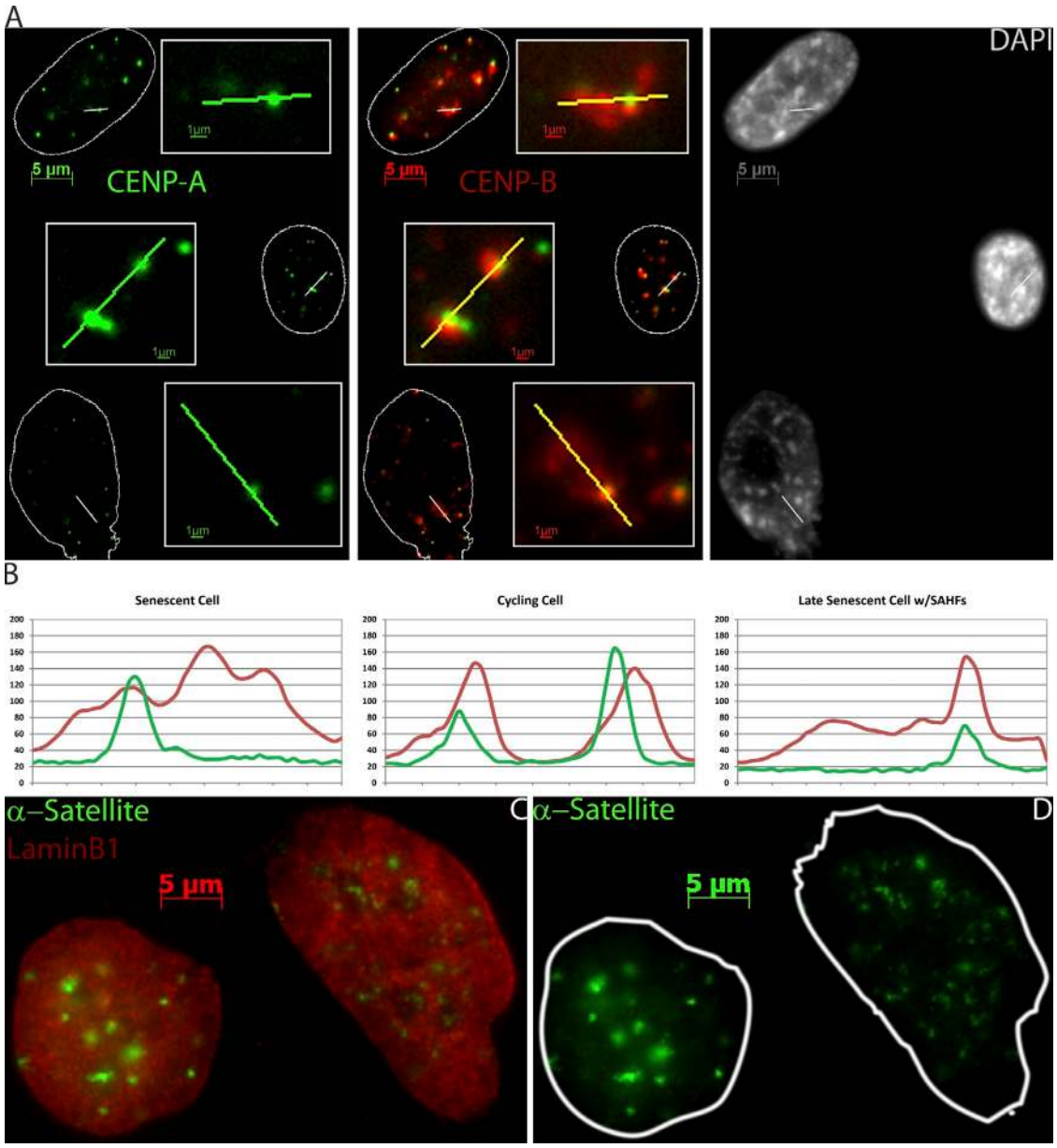

Figure S2. **CENP-A and -B distribution on individual centromeres of senescent cells and LaminB1 levels in cycling and senescent cells.** (A) CENP-A and -B staining in a senescent cell (top), cycling cell (middle), and late senescent cell with prominent SAHF (bottom). CENP-B staining distends in senescent cells (red), whereas CENP-A (green) does not. CENP-A staining levels on individual centromeres showed some variability, but were generally brighter in cycling and early senescent cells (middle and top) than late senescent cells (bottom). This is quantified by a line scan (expanded regions in A) shown in B where signal intensities (CENP-A, green; CENP-B, red) are plotted along the length of the drawn line. (C and D) LaminB1 (red) levels are not always lower in cells with distended satellites (green).

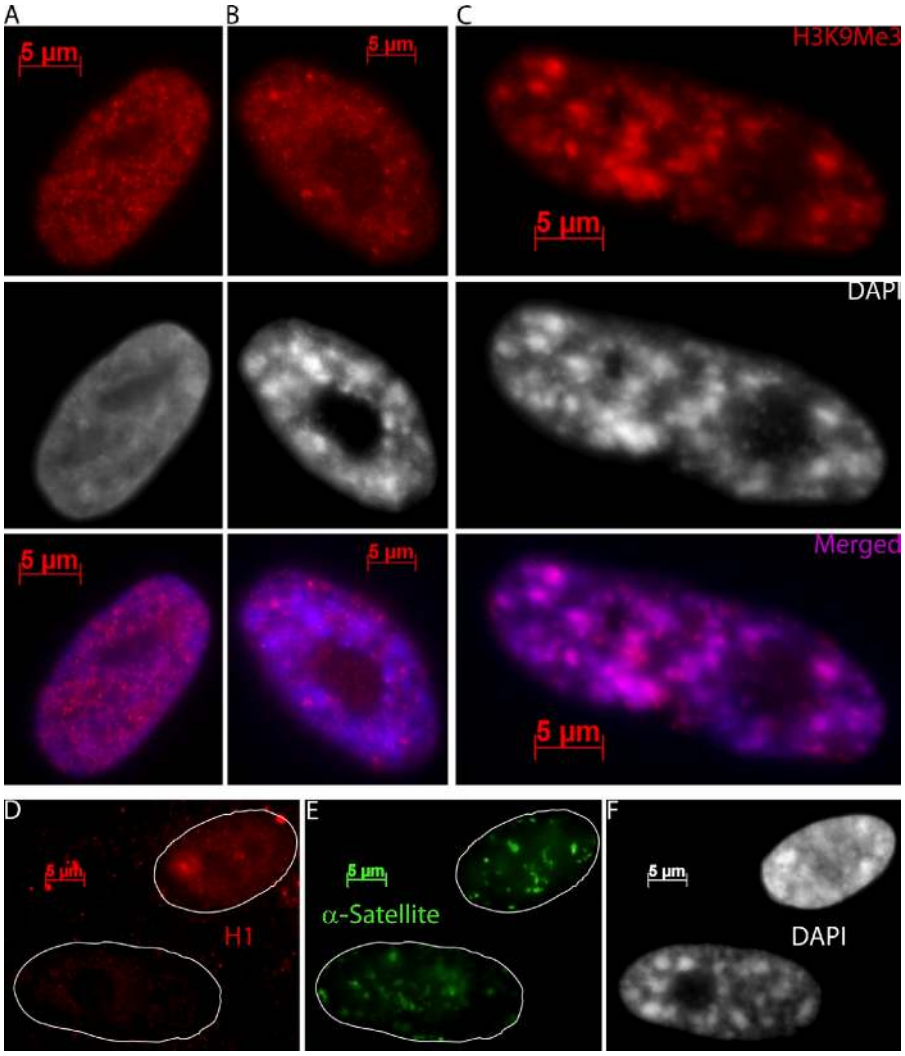

Figure S3. **H3K9Me3 distribution changes and H1 levels decrease with senescence.** H3K9Me3 (red) has a general nucleoplasmic signal in cycling (A, top) and senescent cells (B, middle). H3K9Me3 overlaps SAHF (DAPI) in late senescent cells (C, right). (D–F) Although both cells have distended α-sat (green), the top cell lacks SAHF (DAPI) and has robust H1 staining (red; 64%) and the bottom cell has SAHF and severely diminished H1 staining.

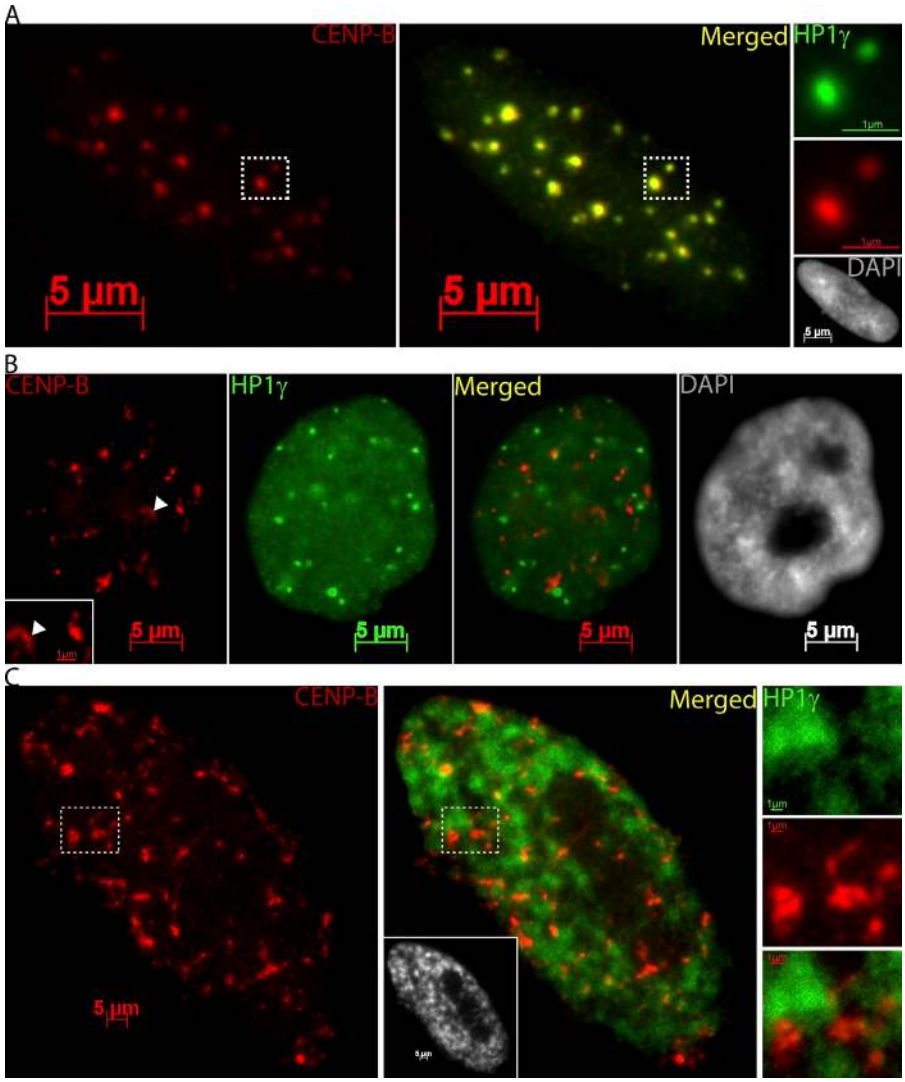

Figure S4. **HP1γ redistributes from satellites to SAHF as cells undergo senescence.** (A and B) HP1γ (green) and CENP-B (red) colocalize in cycling cells with condensed centromeres (A) but not in cells with distended centromeres (B) in which HP1γ gathers at PML bodies and no longer colocalizes with the centromeres. The arrowhead indicates a particularly decondensed centromere (magnified in the inset). The merged image in B combines two different planes. (C) In late stage senescent cells, HP1γ colocalizes with SAHF (DAPI; gray inset) and centromeres are often found in areas that lack intense HP1γ staining (magnified on right).

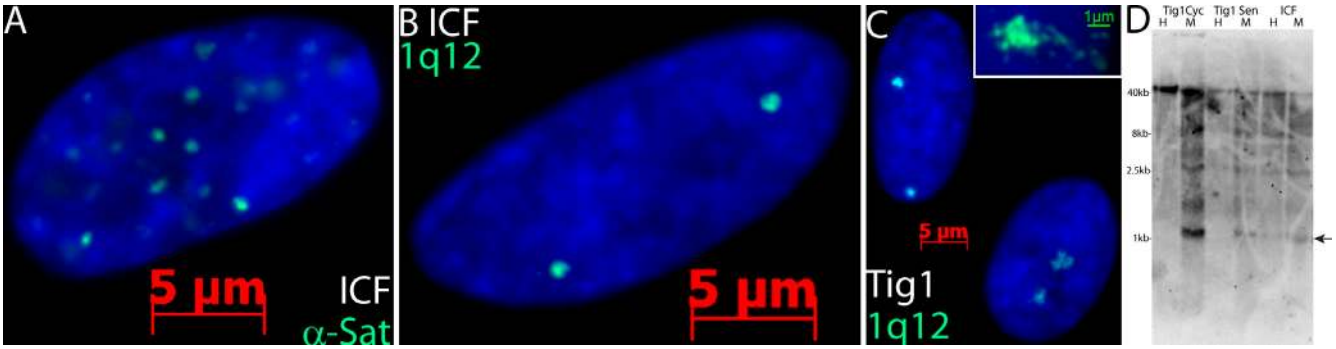

Figure S5. **Effects of hypomethylation on satellite distension.** (A and B) Cycling ICF cells do not display SADS or marked distension of nuclear α-sat (A) or sat II (B) on 1q12. (C) Appearance of sat II 1q12 (green) signals that distend in senescent Tig1 fibroblasts (bottom right), but are compact in cycling cells (top left). The inset shows a separate senescent cell with 1q12 signal that extends to the nuclear periphery. (D) A DNA methylation-sensitive Southern blot with ICF, senescent Tig1, and cycling Tig1 cells digested by HpaII (H) or MspI (M) and detected with a probe for sat II 1q12 sequences. The arrow points to a band size that is lacking in some of the methylation-sensitive HpaII lanes, indicating that the 1q12 region is methylated in the corresponding cell types. It is important to note that 1q12 remains methylated in both cycling and senescent cells.

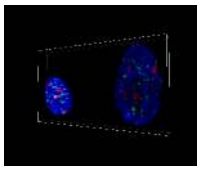

Video 1. **A 3D rendering of Fig. 1 A.** The video depicts a 3D reconstruction of Fig. 1 A created using Axiovision software where a cycling (left) and senescent (right) cell are hybridized with α-sat (green) and sat II (red) in DAPI-stained nuclei.

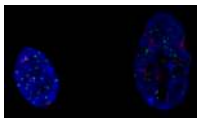

Video 2. **A Z stack from Fig. 1 A.** A cycling (left) and senescent (right) cell hybridized with α-sat (green) and sat II (red) in DAPI-stained nuclei. Each frame correlates to a successive slice (~0.1–0.25-μm apart) in the Z stack obtained with Axiovision software.